

DISCONTINUITIES OF THE INTEGRATED DENSITY OF STATES FOR LAPLACIANS ASSOCIATED WITH PENROSE AND AMMANN–BEENKER TILINGS

DAVID DAMANIK, MARK EMBREE, JAKE FILLMAN, AND MAY MEI

ABSTRACT. Aperiodic substitution tilings provide popular models for quasicrystals, materials exhibiting aperiodic order. We study the graph Laplacian associated with four tilings from the mutual local derivability class of the Penrose tiling, as well as the Ammann–Beenker tiling. In each case we exhibit locally-supported eigenfunctions, which necessarily cause jump discontinuities in the integrated density of states for these models. By bounding the multiplicities of these locally-supported modes, in several cases we provide concrete lower bounds on this jump. These results suggest a host of questions about spectral properties of the Laplacian on aperiodic tilings, which we collect at the end of the paper.

CONTENTS

1. Introduction	1
2. Preliminaries	5
3. Boats and Stars	8
4. Triangles	15
5. Rhombi	18
6. Kites and Darts	23
7. Ammann–Beenker	26
8. Questions and Open Problems	30
References	35

Keywords: Laplacians on aperiodic tilings, eigenvalue computations, locally-supported eigenfunctions, quasicrystals

1. INTRODUCTION

1.1. Prologue. The structure of ordered materials such as crystals has long been a topic of fascination in mathematics and science. The discovery of quasicrystals in the 1980s ushered in new techniques and motivations for investigating aperiodic structures with underlying symmetries. Following this discovery, the study of electronic transport properties of particles in quasicrystalline media has become a fundamental question in mathematics and physics.

Since their discovery in the 1980s by Shechtman *et al.* [29], quasicrystals have generated substantial interest in mathematical physics. For a sample of the mathematical literature devoted to quasicrystals and the mathematics of aperiodic order, see [2, 3, 4, 14, 22, 27] and references therein. Given the physical origins of these models, there has naturally been interest in the analysis of quantum mechanical systems associated with quasicrystals. As such, many researchers have studied spectral problems associated with self-adjoint operators that inherit their structure from a mathematical model of a quasicrystal. From this perspective, one-dimensional quasicrystal models have been discussed extensively, since those models enjoy the largest variety of tools in the spectral toolbox. Particularly refined results have been obtained for the Fibonacci Hamiltonian, the most prominent one-dimensional quasicrystal model; see, e.g., [5, 17, 25, 30, 31] and references therein.

The Penrose tiling is a two-dimensional structure that shares many features with quasicrystals discovered in nature, such as five-fold rotational symmetry and the pure point nature of suitable diffraction measures associated with the tiling [2, 8, 10, 13]. Despite a substantial amount of interest from mathematics and physics, there are relatively few results about the spectral theory of Laplacians on the Penrose tiling, due to the disappearance of some of the crucial tools used in the analysis of one-dimensional quasicrystals. One surprising spectral phenomenon that these operators can exhibit is the presence of locally-supported eigenfunctions. It is known that such locally-supported eigenfunctions can never occur for finite-range operators on $\ell^2(\mathbb{Z}^d)$.

One can construct Laplacians from tilings in two different ways: hopping between tiles and hopping between vertices. We distinguish these paradigms as the “tile model” and the “vertex model,” respectively. For both the tile and the vertex model associated with the rhombus tiling, the presence of locally-supported eigenfunctions was observed in the 1980s [1, 9, 16]. Several other prominent tilings (Robinson triangle, boat–star, and kite–dart) are equivalent to the Penrose tiling, in the sense of mutual local derivability (MLD). On one hand, the presence of finitely supported eigenfunctions depends very sensitively on the local structure of the tiling on which one studies the Laplacian, and hence one would not expect the existence of such eigenfunctions to hold universally in a given MLD class, since the MLD relation can alter the local structure of a tiling. Nevertheless, we study four tilings which are in the MLD class of the Penrose tiling and show that all of them exhibit locally-supported eigenfunctions (and hence exhibit a discontinuous IDS). More recently, vertex models associated with the Penrose and Ammann–Beenker tiling were studied in [21, 23, 24]. We study the tile model for the Ammann–Beenker tiling (also called the octagonal tiling), showing that it too exhibits locally-supported eigenfunctions.

1.2. Setting and Results. Let us now define the relevant objects and state our results. We will work with Laplacians on graphs associated with tilings. A *graph* $\Gamma = (\mathcal{V}, \mathcal{E})$ consists of a nonempty set \mathcal{V} of *vertices* and a set \mathcal{E} comprised of unordered pairs of elements of \mathcal{V} . We write $u \sim v$ if $(u, v) \in \mathcal{E}$ and say that u

and v are *connected* by an edge. The *degree* of v is the number of neighbors of v : $\deg(v) = \#\{u : u \sim v\}$.

The *Laplacian* on the graph $\Gamma = (\mathcal{V}, \mathcal{E})$ is the operator

$$\Delta = \Delta_\Gamma : \ell^2(\mathcal{V}) \rightarrow \ell^2(\mathcal{V}), \quad [\Delta\psi](v) = \sum_{u \sim v} (\psi(v) - \psi(u)).$$

Equivalently, one can define $\Delta = \mathcal{D} - \mathcal{A}$, where \mathcal{D} is the degree operator and \mathcal{A} is the adjacency operator:

$$\begin{aligned} [\mathcal{D}\psi](v) &= \deg(v)\psi(v) \\ [\mathcal{A}\psi](v) &= \sum_{u \sim v} \psi(u). \end{aligned}$$

We are interested in infinite graphs that arise from substitution tilings of the plane by polygons. Namely (once a tiling of the plane by polygons has been constructed), the associated graph has one vertex for each polygon of the tiling, and two vertices are connected if the associated polygons share at least one edge.

One fruitful way to study such infinite graphs is to analyze finite truncations. Namely, one may consider finite subsets $\mathcal{V}_n \subseteq \mathcal{V}$ and $\mathcal{E}_n = \{(u, v) : u, v \in \mathcal{V}_n\}$ with $\mathcal{V}_n \uparrow \mathcal{V}$ in a suitable sense, and let $\Delta_n := \Delta_{\Gamma_n}$ denote the Laplacian on the finite graph $\Gamma_n = (\mathcal{V}_n, \mathcal{E}_n)$. The normalized eigenvalue counting measure is given by

$$(1.1) \quad \nu_n(B) = \frac{1}{\#\mathcal{V}_n} \text{Tr} \chi_B(\Delta_n), \quad B \subseteq \mathbb{R} \text{ measurable.}$$

Under suitable assumptions (which are met in all of the cases under consideration in the present work), ν_n converges in the weak* sense to a limiting measure

$$(1.2) \quad \nu = \nu_\Gamma,$$

which we call the *density of states measure* (DOSM) of the graph Γ , and the limit is independent on the choice of $\{\mathcal{V}_n\}_{n=1}^\infty$; this is described in more detail in [18, 19, 20].

The *integrated density of states* of Γ is the accumulation function of the measure ν_Γ :

$$(1.3) \quad k_\Gamma(E) = \nu_\Gamma((-\infty, E]).$$

One is then naturally interested in regularity properties of this function: is it continuous on suitable intervals, and if so, what can one say about the modulus of continuity there, and so on.

Here, we study questions of this kind for various versions of the *Penrose tiling*.

Notation 1.1. We use Γ_\star , Γ_\blacktriangle , Γ_\blacklozenge , Γ_\blackspade , Γ_\blacksquare to refer to the graphs of the boat–star tiling, the Robinson triangle tiling, the rhombus tiling, the kite–dart tiling, and the Ammann–Beenker tiling respectively. For ease of notation, we drop the Γ when referring to the corresponding integrated density of states as k_\star , k_\blacktriangle , k_\blacklozenge , k_\blackspade , and k_\blacksquare .

Theorem 1.2. *If $\square \in \{\star, \blacktriangle, \blacklozenge, \blackspade\}$, then the integrated density of states k_\square is discontinuous.*

A similar result holds for the *Ammann–Beenker tiling*.

Theorem 1.3. *The integrated density of states k_{\blacksquare} is discontinuous.*

We direct the reader to later sections for precise definitions of these tilings.

The tilings that we discuss are linearly repetitive (see, e.g., [2] for the definition and a discussion of this concept): in particular, any pattern that is observed once is observed infinitely often with positive frequency. In view of (1.1), (1.2), and (1.3), a locally-supported eigenfunction necessarily produces a discontinuity of the IDS at the corresponding eigenvalue. More precisely, if Δ_{Γ} enjoys an eigenvalue E with an eigenfunction having local support, then (a one-tile neighborhood of) the support of the eigenfunction occurs with positive frequency, and hence one observes a jump discontinuity in k_{Γ} . In fact, it is known that (under suitable assumptions on the underlying graph) a discontinuity of the IDS at energy E is *equivalent* to the presence of a locally-supported eigenfunction with eigenvalue E [15].

Furthermore, with this picture, one can estimate the size of the jump discontinuity by estimating the frequency with which the support of the eigenfunction occurs. Concretely, we can sharpen the conclusions of Theorem 1.2 in some individual cases. Here is a representative selection of theorems that one can prove.

Theorem 1.4. *If Γ is a graph associated with the boat–star tiling,*

$$(1.4) \quad k_{\star}(4+) - k_{\star}(4-) \geq \frac{65 - 29\sqrt{5}}{10} \approx 0.01540\dots$$

Theorem 1.5. *If Γ is a graph associated with the Robinson triangle tiling,*

$$(1.5) \quad k_{\blacktriangle}(E+) - k_{\blacktriangle}(E-) \geq \frac{65 - 29\sqrt{5}}{20} \approx 0.007701\dots, \quad E \in \{2, 4\}.$$

Theorem 1.6. *If Γ is a graph associated with the Ammann–Beenker tiling,*

$$(1.6) \quad k_{\blacksquare}(4+) - k_{\blacksquare}(4-) \geq 1270 - 898\sqrt{2} \approx 0.036221\dots,$$

$$(1.7) \quad k_{\blacksquare}(6+) - k_{\blacksquare}(6-) \geq 116 - 82\sqrt{2} \approx 0.0344879\dots$$

Remark 1.7. Let us make some remarks about these theorems.

- (a) Since the frequency calculations are somewhat similar in the different examples, we do not discuss quantitative estimates in all cases, but rather focus on a representative subset of examples. An estimate for the lower bound on the jump in the IDS for the rhombus tiling is discussed in [9]. The jump discontinuity for the kite–dart tiling may be estimated similarly to the others.
- (b) One may naturally be interested in whether the bounds are sharp, that is, whether the jump in the IDS is precisely given by the enumerated expressions. Let us comment on the difficulties associated with “the other direction.” The lower bounds are computed by (1) identifying patterns in a given tiling that can support a finitely-supported eigenfunction and (2) finding combinatorial mechanisms in the substitution structure generating the tiling that enable us to estimate the frequency with which the desired pattern(s)

occur. Thus, if one wishes to prove that the estimates are sharp, one must overcome two obstacles:

- (1) One must show that one has identified all pattern(s) in the tiling that permit a finitely-supported eigenfunction with the desired energy.
- (2) One must show that the pattern(s) that one has identified can only arise via the combinatorial mechanisms that one used to estimate the frequency.

The second obstacle can likely be overcome with a sufficiently careful analysis of suitably large supertiles. However, the first obstacle appears to be genuinely intractable with current technology. (Indeed, Figures 13 and 24 show eigenfunctions with large-but-finite support that emerge on larger tilings, and cannot be expressed as linear combinations of our simpler eigenfunctions supported on small patches.)

One crucial point that we want to emphasize is the synergy between the numerical and spectral analyses. The eigenfunctions discussed in this paper were first discovered via numerical spectral computations on finite graph Laplacians Δ_n . Given the finite nature of the sought-after eigenfunctions, such numerical calculations (once carried out on a sufficiently large finite patch) suffice to demonstrate the existence of finitely supported eigenfunctions and discontinuities of the IDS. Once found, simple locally-supported modes can readily be verified by hand. However for some tilings, larger graphs reveal additional eigenfunctions whose local support extends to several hundred tiles, making manual calculations inadvisable.

In addition to suggesting theorems, numerics can also provide evidence for new conjectures. In that spirit, we will conclude the paper with numerical plots of large finite-volume approximations of the integrated densities of states associated with these tilings, and pose some interesting open problems suggested by this work.

Acknowledgements. The authors thank Michael Baake, Semyon Dyatlov, and Anton Gorodetski for many helpful conversations and the American Institute of Mathematics for hospitality and support through the SQuaRE program during a remote meeting in January 2021 and a January 2022 visit, during which part of this work was completed. D.D. was supported in part by NSF grants DMS-1700131 and DMS-2054752, and Simons Fellowship #669836. M.E. was supported in part by NSF grant DMS-1720257. J.F. was supported in part by NSF grant DMS-2213196 and Simons Foundation Collaboration grant #711663.

2. PRELIMINARIES

2.1. Tilings and Associated Laplacians. To set the stage and fix notation, let us recall some notation, conventions, and definitions largely following Baake–Grimm [2].

Definition 2.1 (Patterns, Fragments, and Tiles). A *pattern* $\mathcal{T} = \{T_i : i \in I\}$ in \mathbb{R}^2 is a nonempty set whose elements T_i are nonempty subsets of \mathbb{R}^2 . We write $\mathcal{T} \sqsubset \mathbb{R}^2$ to denote that \mathcal{T} is a pattern in \mathbb{R}^2 and say \mathcal{T} is a *tiling* if I is countable, the T_i

are closed and nonempty sets, $\bigcup_{i \in \mathbb{Z}} T_i = \mathbb{R}^2$, and $T_i^\circ \cap T_j^\circ = \emptyset$ for all $i \neq j$. The elements T_i of \mathcal{T} are called *tiles* or *fragments* of \mathcal{T} .

In the sequel, we will occasionally want to distinguish tiles that are the same as subsets of \mathbb{R}^2 but that nevertheless have different behavior under substitution rules. For instance, the reader may consider the example below in Definition 2.4, in which there are two basic tile shapes (acute and obtuse triangles), but two different colors of each shape (each of which behaves as the mirror image of the other under substitutions). One often uses colors or decorations to distinguish between different types of the same shape. By abuse of notation, we will still refer to tilings with colors or decorations as *tilings* rather than *decorated tilings*.

For $\mathcal{T} \sqsubset \mathbb{R}^2$ and $K \subseteq \mathbb{R}^2$, $\mathcal{T} \sqcap K$ is the pattern consisting of all fragments of \mathcal{T} that intersect K nontrivially:

$$\mathcal{T} \sqcap K := \{T_i : T_i \in \mathcal{T} \text{ and } T_i \cap K \neq \emptyset\}.$$

Naturally, for $\mathcal{T} \sqsubset \mathbb{R}^2$ and $t \in \mathbb{R}^2$, the *translation* of \mathcal{T} by t is given by

$$t + \mathcal{T} = \{t + T_i : T_i \in \mathcal{T}\}.$$

We refer to the equivalence class of tiles up to translation as *prototiles*. Finally, given patterns $\mathcal{T}_0 \subseteq \mathcal{T} \sqsubset \mathbb{R}^2$, an *occurrence* of \mathcal{T}_0 in \mathcal{T} is any translation of \mathcal{T}_0 that is also a subset of \mathcal{T} ; in other words, an occurrence of \mathcal{T}_0 is any arrangement of tiles in \mathcal{T} that looks the same as \mathcal{T}_0 , up to translation.

The pattern $\mathcal{T}' \sqsubset \mathbb{R}^2$ is said to be *locally derivable* from $\mathcal{T} \sqsubset \mathbb{R}^2$ (denoted $\mathcal{T} \xrightarrow{\text{LD}} \mathcal{T}'$) if for some $R > 0$ one has

$$(-x + \mathcal{T}) \sqcap B_R = (-y + \mathcal{T}) \sqcap B_R \implies (-x + \mathcal{T}') \sqcap \{0\} = (-y + \mathcal{T}') \sqcap \{0\},$$

where B_R denotes the open ball of radius R centered at the origin (note that equality of patterns includes equality of colors as well). If $\mathcal{T} \xrightarrow{\text{LD}} \mathcal{T}'$ and $\mathcal{T}' \xrightarrow{\text{LD}} \mathcal{T}$, we say that \mathcal{T} and \mathcal{T}' are *mutually locally derivable* (MLD) and denote this by $\mathcal{T} \xleftrightarrow{\text{MLD}} \mathcal{T}'$.

Definition 2.2. A *polygon* is a nonempty compact subset \mathbb{R}^2 with dense interior obtained by intersecting finitely many closed half-planes. From this point onward, all tiles are assumed to be polygonal. Let $\mathcal{T} = \{T_i : i \in I\}$ be such a tiling of \mathbb{R}^2 . The *induced graph* $\Gamma = \Gamma_{\mathcal{T}} = (\mathcal{V}, \mathcal{E})$ has $\mathcal{V} = I$ and one has $u \sim v$ if and only if T_u and T_v share at least one edge. The associated *Laplace operator* acts on the space $\mathcal{H} = \ell^2(\mathcal{V})$ via

$$(2.1) \quad [\Delta\psi](v) = \sum_{u \sim v} (\psi(u) - \psi(v)) \quad \psi \in \ell^2(\mathcal{V}).$$

2.2. Substitution Tilings. Let us now describe the main setting in which we work: tilings that are generated by a substitution rule.

Definition 2.3 (Substitution Tilings). Let $\mathcal{P} = \{P_1, \dots, P_n\}$ denote a finite *proto-set*, or collection of prototiles in \mathbb{R}^2 . Denote by \mathcal{P}^* the collection of finite patterns $\mathcal{T} \sqsubset \mathbb{R}^2$ whose elements are images of elements of \mathcal{P} under translation and rotation.

A *substitution* is a map $S : \mathcal{P} \rightarrow \mathcal{P}^*$. One can extend S to \mathcal{P}^* in a natural manner, so we can speak of iterates of S .

A *substitution tiling* associated with S is a polygonal tiling \mathcal{T} such that any finite patch of \mathcal{T} occurs in $S^n(P)$ for some $P \in \mathcal{P}$ and some $n \in \mathbb{N}$. The collection \mathbb{X}_S of all such tilings is called the *hull* of S and is a compact set in a suitable tiling metric. Since it is not central to our work, we will not specify the tiling metric precisely, but we simply say that two tilings are close in the tiling metric if after a small shift they coincide on a large ball centered at the origin. Clearly \mathbb{R}^2 acts on \mathbb{X}_S by translations. It is known that for suitable substitutions, this translation action is *minimal* (i.e., the translation orbit of any element of \mathbb{X}_S is dense in \mathbb{X}_S).

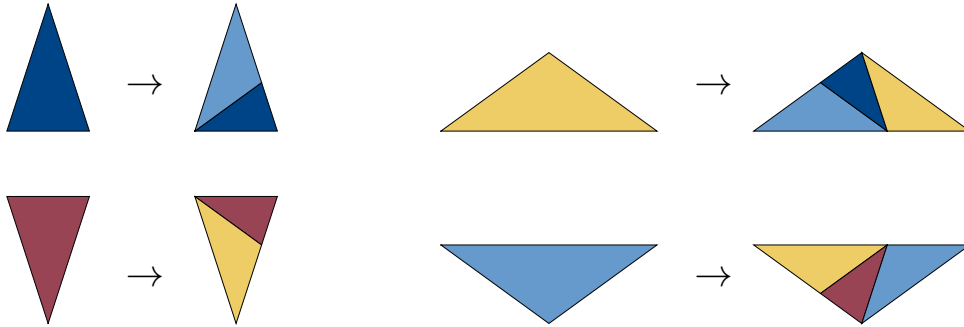
Given a substitution S on a set \mathcal{P} as above, the associated *substitution matrix* is the $n \times n$ matrix M whose entry in row i and column j is the number of occurrences of tile P_i in $S(P_j)$.

In what follows, we will consider five tilings generated by substitution rules. Let us start with an example.

Definition 2.4. The *Robinson triangle substitution* has four basic tiles:



The substitution rules are (redrawing [7, Fig. 13]):



We denote this substitution by S_{\blacktriangle} . Abusing notation somewhat, we write $M_{\blacktriangle} := M_{S_{\blacktriangle}}$ for its substitution matrix. Ordering the tiles from left-to-right as above,

$$M_{\blacktriangle} = \begin{bmatrix} 1 & 1 & 0 & 0 \\ 0 & 1 & 1 & 1 \\ 0 & 0 & 1 & 1 \\ 1 & 1 & 0 & 1 \end{bmatrix}.$$

Recall that the graph $\Gamma = (\mathcal{V}, \mathcal{E})$ associated with a tiling $\mathcal{T} = \{T_i : i \in I\}$ has vertex set $\mathcal{V} = \{T_i : i \in I\}$ and edges between two vertices if and only if the corresponding tiles share an edge.

Let us now describe more precisely the mechanism that enables one to estimate the discontinuity in the IDS. The following result is well known, but we make it explicit for the reader's benefit. Throughout this discussion, fix a substitution tiling \mathcal{T} and associated graph $\Gamma = (\mathcal{V}, \mathcal{E})$. If $\mathcal{V}_0 \subseteq \mathcal{V}$ is a finite patch, we denote its boundary by $\partial\mathcal{V}_0$, which consists of all the tiles in \mathcal{V}_0 that share an edge with a tile in $\mathcal{V} \setminus \mathcal{V}_0$. A priori, one may be concerned that the degree of the tiles in $\partial\mathcal{V}_0$ are ill-defined. In the specific patches we consider in this paper, one may verify directly that this is not the case.

Definition 2.5. We say $P \subseteq \mathcal{V}$ is a *good eigenfunction support* at energy E if

- (1) P is finite;
- (2) there is a nontrivial eigenfunction ψ of Δ_Γ with $\Delta_\Gamma\psi = E\psi$ and $\text{supp}(\psi) = P$;
- (3) no proper subset of P enjoys the previous property;
- (4) every occurrence of P in \mathcal{V} supports an eigenfunction.

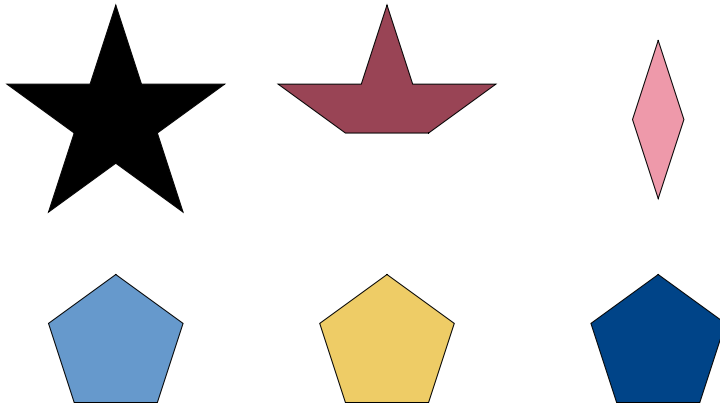
Proposition 2.6. *Suppose $P \subseteq \mathcal{V}$ is a good eigenfunction support at energy E . For any finite patch $\Gamma_0 = (\mathcal{V}_0, \mathcal{E}_0)$, $\mathcal{V}_0 \subseteq \mathcal{V}$, the multiplicity of E for Δ_{Γ_0} is bounded from below by the largest cardinality of a set of occurrences of P in \mathcal{V}_0 with the following properties: no occurrence intersects $\partial\mathcal{V}_0$ and no occurrence is contained in the union of other occurrences.*

Proof. Choose a collection of occurrences of P having the enumerated properties. The definitions ensure that each occurrence of P yields an eigenfunction and that the collection of these eigenfunctions is linearly independent. \square

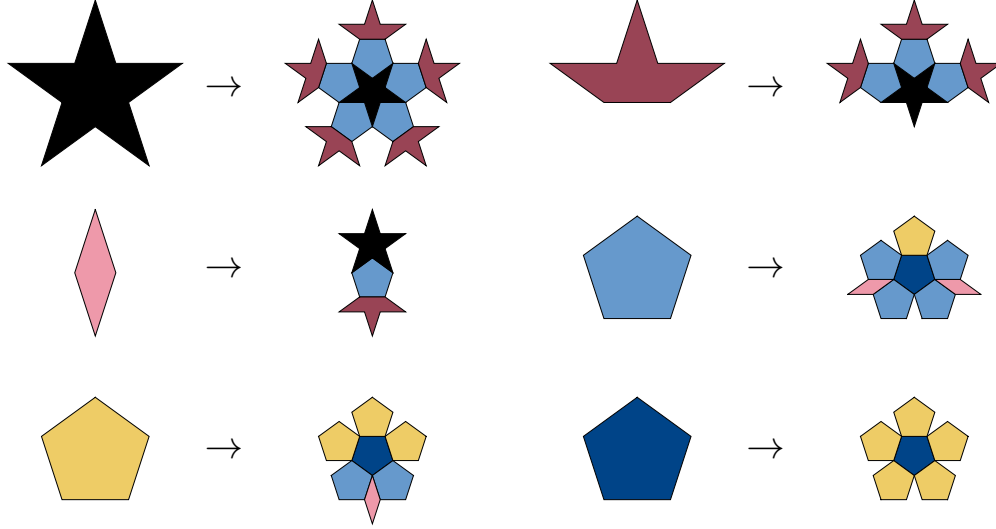
3. BOATS AND STARS

3.1. Basics.

Definition 3.1. Following [13], the *boat-star substitution* has six basic tiles:



The substitution rules are:



We denote this substitution by S_{\star} .

There are six tiles: stars, boats, diamonds, and three types of pentagons. Ordering the tiles as in Definition 3.1, one can see that the substitution matrix for the boat–star substitution is

$$M_{\star} = \begin{bmatrix} 1 & 1 & 1 & 0 & 0 & 0 \\ 5 & 3 & 1 & 0 & 0 & 0 \\ 0 & 0 & 0 & 2 & 1 & 0 \\ 5 & 3 & 1 & 4 & 2 & 0 \\ 0 & 0 & 0 & 1 & 3 & 5 \\ 0 & 0 & 0 & 1 & 1 & 1 \end{bmatrix}.$$

Let \mathcal{T}_0^{\star} denote the pattern consisting of a single star tile and $\mathcal{T}_n^{\star} = S_{\star}^n(\mathcal{T}_0^{\star})$. Denote the golden ratio by

$$\varphi = \frac{\sqrt{5} + 1}{2}.$$

Lemma 3.2. *For each $n \geq 0$, the total number of tiles in \mathcal{T}_n^{\star} is*

$$P_{\star}(n) = \frac{1}{22}(25 + 9\sqrt{5})\varphi^{4n} - \frac{5}{33}4^{n+1} - \frac{2}{3} + \frac{1}{22}(25 - 9\sqrt{5})\varphi^{-4n},$$

of which precisely

$$P_{\text{pent}}(n) = \frac{1}{22}(17 + 7\sqrt{5})\varphi^{4n} - \frac{40}{33}4^n - \frac{1}{3} + \frac{1}{22}(17 - 7\sqrt{5})\varphi^{-4n}$$

are pentagons.

Proof. Observe that the substitution matrix M_\star has eigenvalues $\varphi^4, 4, 1, \varphi^{-4}, 0, 0$ with corresponding eigenfunctions (listed in the same order)

$$v_1 = \frac{1}{2} \begin{bmatrix} 3 - \sqrt{5} \\ -5 + 3\sqrt{5} \\ 5 - \sqrt{5} \\ 5 + \sqrt{5} \\ 2\sqrt{5} \\ 2 \end{bmatrix}, \quad v_2 = \begin{bmatrix} -1 \\ -4 \\ 1 \\ -2 \\ 8 \\ 2 \end{bmatrix}, \quad v_3 = \begin{bmatrix} 1 \\ -5 \\ 5 \\ 5 \\ -5 \\ 1 \end{bmatrix},$$

$$v_4 = \frac{1}{2} \begin{bmatrix} 3 + \sqrt{5} \\ -5 - 3\sqrt{5} \\ 5 + \sqrt{5} \\ 5 - \sqrt{5} \\ -2\sqrt{5} \\ 2 \end{bmatrix}, \quad v_5 = \begin{bmatrix} 1 \\ -2 \\ 1 \\ 0 \\ 0 \\ 0 \end{bmatrix}, \quad v_6 = \begin{bmatrix} 0 \\ 0 \\ 0 \\ 1 \\ -2 \\ 1 \end{bmatrix}.$$

Since the tiling begins with a single star, the total number of tiles at stage n is precisely $\langle w, M_\star^n e_1 \rangle$ where $w = [1 \ 1 \ 1 \ 1 \ 1 \ 1]^\top$. Decomposing e_1 in the basis of eigenfunctions of M_\star , one observes

$$e_1 = \frac{1}{22}(7 - \sqrt{5})v_1 - \frac{5}{33}v_2 - \frac{1}{3}v_3 + \frac{1}{22}(7 + \sqrt{5})v_4.$$

Calculate

$$\langle w, v_1 \rangle = 5 + 2\sqrt{5}, \quad \langle w, v_2 \rangle = 4, \quad \langle w, v_3 \rangle = 2, \quad \langle w, v_4 \rangle = 5 - 2\sqrt{5}.$$

Thus, the total number of tiles at stage n is

$$\begin{aligned} \langle w, M_\star^n e_1 \rangle &= \frac{1}{22}(7 - \sqrt{5})(5 + 2\sqrt{5})\varphi^{4n} - \frac{5}{33}4^{n+1} - \frac{2}{3} + \frac{1}{22}(7 + \sqrt{5})(5 - 2\sqrt{5})\varphi^{-4n} \\ &= \frac{1}{22}(25 + 9\sqrt{5})\varphi^{4n} - \frac{5}{33}4^{n+1} - \frac{2}{3} + \frac{1}{22}(25 - 9\sqrt{5})\varphi^{-4n}. \end{aligned}$$

Similarly, to count pentagons let $u = [0 \ 0 \ 0 \ 1 \ 1 \ 1]^\top$ and compute

$$\langle u, v_1 \rangle = \frac{1}{2}(7 + 3\sqrt{5}), \quad \langle u, v_2 \rangle = 8, \quad \langle u, v_3 \rangle = 1, \quad \langle u, v_4 \rangle = 7 - 3\sqrt{5}.$$

Thus, the total number of pentagons at stage n is

$$\begin{aligned} \langle u, M_\star^n e_1 \rangle &= \frac{1}{22}(7 - \sqrt{5})\frac{1}{2}(7 + 3\sqrt{5})\varphi^{4n} - \frac{40}{33}4^n - \frac{1}{3} + \frac{1}{22}(7 + \sqrt{5})\frac{1}{2}(7 - 3\sqrt{5})\varphi^{-4n} \\ &= \frac{1}{22}(17 + 7\sqrt{5})\varphi^{4n} - \frac{40}{33}4^n - \frac{1}{3} + \frac{1}{22}(17 - 7\sqrt{5})\varphi^{-4n}, \end{aligned}$$

as desired. \square

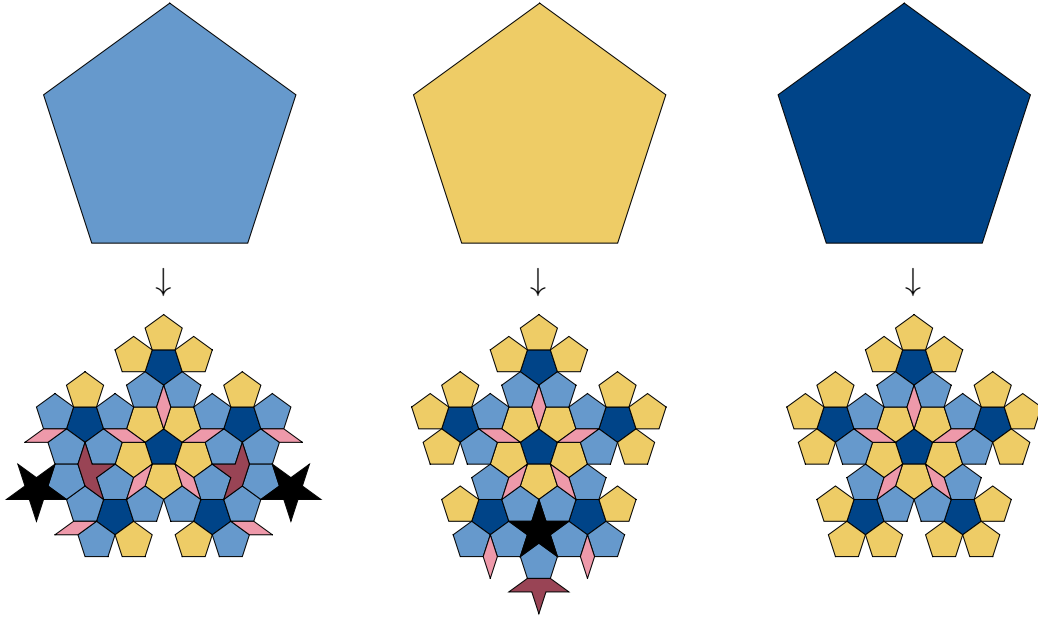


FIGURE 1. Pentagonal supertiles at level 2 (i.e., \mathcal{T}_2^κ for each color κ).

3.2. Ring Modes. We now explain how the locally-supported eigenfunctions arise and how to estimate their frequency. For each of the three colors κ , let \mathcal{T}_0^κ denote the pattern that consists of a single pentagon with color κ , let $\mathcal{T}_n^\kappa = S_\star^n(\mathcal{T}_0^\kappa)$ denote the result of substituting n times, let Γ_n^κ denote the induced finite graph, and denote the corresponding graph Laplacian by Δ_n^κ . We will refer to \mathcal{T}_n^κ as a *level- n pentagonal supertile*. See Figure 1 for the three level-two pentagonal supertiles.

The crucial observation is that each level-two pentagonal supertile contains a pattern that supports a locally-supported eigenfunction. Namely, the ring of ten

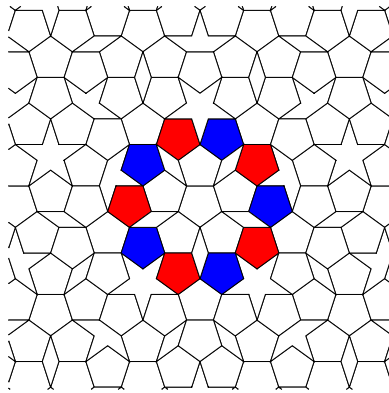


FIGURE 2. A locally-supported eigenfunction for $E = 4$ on the boat-star tiling. The function takes the value $+1$ on blue tiles, -1 on red tiles, and zero elsewhere.

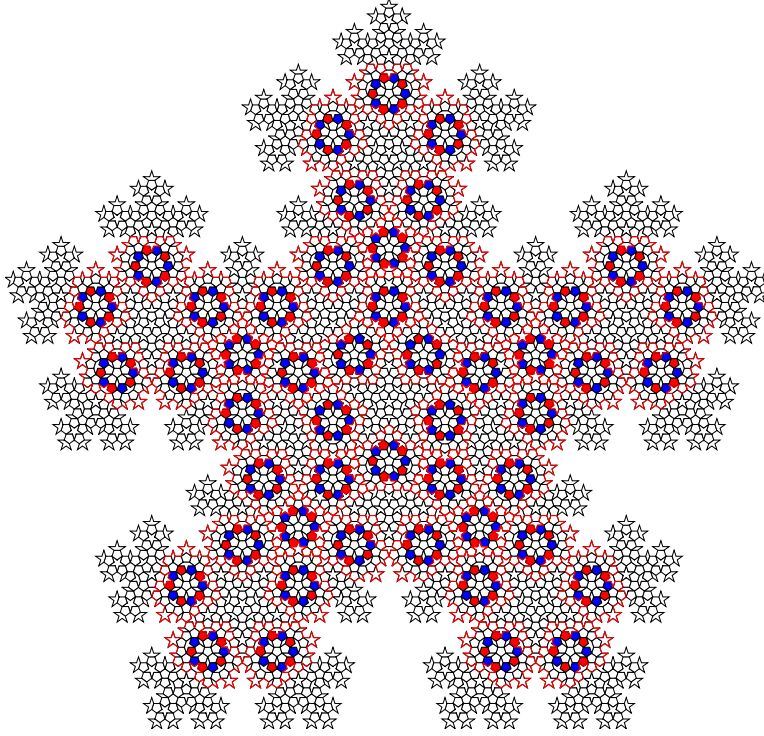


FIGURE 3. Boat–star tiling, level 4, $E = 4$. Fifty locally-supported ring modes: the colored tiles correspond to mode entries equal to ± 1 . The red lines show the boundaries of the fifty pentagonal supertiles (each of which is generated by a pentagon on the level 2 tiling).

pentagons encircling the center is precisely the tile set that can be used to support a locally-supported eigenfunction. One can locate *fifty* level-two pentagonal supertiles in the level-four supertile shown in Figure 3.

Lemma 3.3. *For all κ , 4 is an eigenvalue of Δ_2^κ .*

Proof. Let us begin by explaining how the eigenfunction arises. Consider Figure 1, which shows \mathcal{T}_2^κ for each color κ . In each \mathcal{T}_2^κ , one observes a ring of ten pentagons encircling the center, highlighted in Figure 2. Denote this pattern by \mathcal{R} . Define a vector ψ by assigning the value +1 to each red pentagon, -1 to each blue pentagon, and 0 to all other tiles.

A brief calculation shows $\Delta_2^\kappa \psi = 4\psi$. Indeed, when u corresponds to a face with combinatorial distance 2 from \mathcal{R} , then

$$[\Delta_2^\kappa \psi](u) = 0 = 4\psi(u).$$

Similarly, one checks $[\Delta_2^\kappa \psi](u) = 4\psi(u)$ for any u coming from a face of \mathcal{R} . Each face with combinatorial distance one from \mathcal{R} has precisely two neighbors in \mathcal{R} , so, due to the alternating pattern, one observes

$$[\Delta_2^\kappa \psi](u) = 1 - 1 = 0 = 4\psi(u),$$

hence showing that ψ is an eigenfunction of eigenvalue 4, as desired. \square

Proof of Theorem 1.4. By Lemma 3.3, the number of occurrences of the pattern \mathcal{R} at level n may be bounded from below by the number of pentagons that appear in level $n - 2$.

For instance, in level 3, there are five occurrences of the pattern, each of which is precipitated by a pentagon from \mathcal{T}_1 ; compare Figure 3.

We now make two observations. First, each of these occurrences will be separated by all other occurrences by a tiling distance of at least two.

Second, we need to address a minor technicality. Namely: some of the ring patterns from Lemma 3.3 may appear on the interior of the tiling, while others may occur on the boundary. As can be seen from Figure 1, either occurrence leads to an eigenfunction.

Thus, we see that the multiplicity of the eigenvalue 4 at level n is bounded from below by the number of pentagons that occur in level $n - 2$. Denoting the IDS by k_\star , Lemma 3.2 gives

$$\begin{aligned} k_\star(4+) - k_\star(4-) &\geq \lim_{n \rightarrow \infty} \frac{P_{\text{pent}}(n)}{P(n+2)} \\ &= \lim_{n \rightarrow \infty} \frac{\frac{1}{22}(17 + 7\sqrt{5})\varphi^{4n} + O(4^n)}{\frac{1}{22}(25 + 9\sqrt{5})\varphi^{4(n+2)} + O(4^n)} \\ &= \frac{17 + 7\sqrt{5}}{(25 + 9\sqrt{5})\varphi^8} \\ &= \frac{65 - 29\sqrt{5}}{10}, \end{aligned}$$

as claimed. \square

One might naturally question whether this estimate on the multiplicity is sharp.

Question 3.4. For $n = 1, 2, \dots, 8$, the multiplicity of the eigenvalue 4 for \mathcal{T}_n is given by

$$(3.1) \quad m(n) = \begin{cases} 0, & n = 0, 1; \\ 1, & n = 2; \\ \frac{1}{22}(17 + 7\sqrt{5})\varphi^{4(n-2)} - \frac{40}{33}4^{n-2} - \frac{1}{3} + \frac{1}{22}(17 - 7\sqrt{5})\varphi^{-4(n-2)}, & n \geq 3. \end{cases}$$

Does this pattern persist? That is, is it true that the multiplicity of $E = 4$ at level n is given by $m(n)$ for all $n \geq 1$?

Remark 3.5. Question 3.4 has been answered in the affirmative (numerically) for all $n \leq 8$; compare Table 4. (The single eigenfunction that appears at energy 4 at level 2 is not a ring consisting of ten pentagons, but is qualitatively different; its support comprises thirty tiles, all on the boundary; in contrast to the ring modes,

this pattern does *not* extend to a locally-supported eigenfunction of larger patches of the tiling.)

Table 4 summarizes some results of our computations. In addition to the ring modes at $E = 4$, Table 4 also contains counts for high-multiplicity eigenvalues at $E = 1/\varphi^2$ and $E = \varphi^2$ associated with modes that are locally-supported, but only on the boundary of the finite patch \mathcal{T}_n^\star . Figure 5 shows a few of these boundary modes. Denote by $k_{\star,n}$ the IDS associated with \mathcal{T}_n^\star . The boundary modes outnumber the ring modes at early levels, and will cause a jump in $k_{\star,n}$ at $E = 1/\varphi^2$ and $E = \varphi^2$ that diminishes as the level increases; The jump at $E = 4$ grows with the level, as quantified in Table 4. (Peek ahead to Figure 25 for an illustration.)

TABLE 4. Boat–star tiling: Multiplicities of different eigenvalues at levels 2–8, with a comparison to the conjectured multiplicity of $E = 4$. The final column shows the numerical approximation to the IDS jump at $E = 4$. The theoretically obtained lower bound on $k_{\star}(4+) - k_{\star}(4-)$ from Theorem 1.4 is $(65 - 29\sqrt{5})/10 \approx 0.01540286525\dots$

level	tiles	$E = 1/\varphi^2$	$E = \varphi^2$	$E = 4$	$m(n)$	$k_{\star,n}(4+) - k_{\star,n}(4-)$
1	16	0	0	0	0	0.0000000...
2	86	10	10	1	1	0.0116279...
3	621	30	30	5	5	0.0080515...
4	4371	110	110	50	50	0.0114390...
5	30406	430	430	400	400	0.0131552...
6	210181	1710	1710	2965	2965	0.0141068...
7	1447691	6830	6830	21210	21210	0.0146509...
8	9950966	27310	27310	148920	148920	0.0149653...

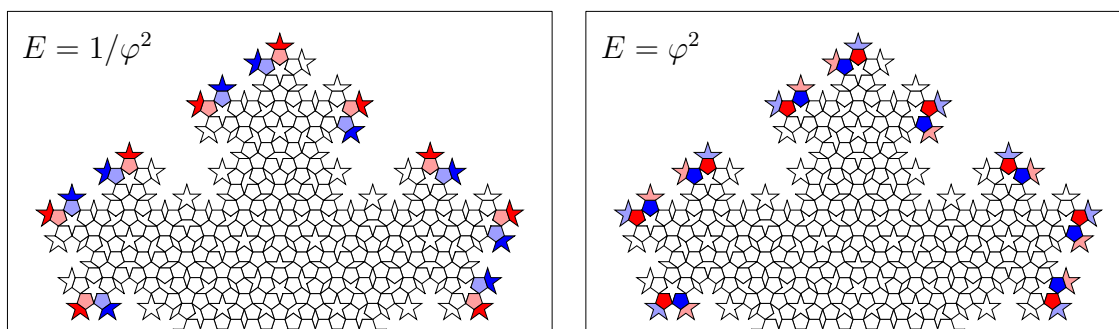


FIGURE 5. Locally-supported boundary eigenfunctions for the boat–star tiling for $E = 1/\varphi^2$ (left) and $E = \varphi^2$ (right) at level 3. Each plot shows nine linearly independent eigenfunctions, each supported on four tiles. The nonzero entries of the eigenfunctions are ± 1 (dark blue and red) and $\pm 1/\varphi$ (light blue and red).

4. TRIANGLES

This section discusses the Robinson triangle substitution, including proofs of the relevant portion of Theorem 1.2, as well as Theorem 1.5. The Robinson triangle part of Theorem 1.2 follows immediately from the observation of a single locally-supported eigenfunction [15]. The bulk of this section is then concerned with the proof of Theorem 1.5, the estimate from below of the discontinuity in the integrated density of states at energies $E = 4$ and $E = 6$.

4.1. Basics. The *Robinson triangle substitution*, denoted S_{\blacktriangle} , was specified in Definition 2.4.

Notation 4.1. We will refer to the acute and obtuse triangles as A and O tiles, respectively.

Let $\mathcal{T}_0^{\blacktriangle}$ denote the pattern consisting of 10 O tiles of oscillating color arranged in a star. We will refer to $\mathcal{T}_n^{\blacktriangle} := S_{\blacktriangle}^n(\mathcal{T}_0^{\blacktriangle})$ as the level- n tiling; see Figure 6.

For $\alpha \in \{A, O\}$, let α_n denote the number of α -type tiles in $\mathcal{T}_n^{\blacktriangle}$. Additionally, let $\{F_n\}_{n=0}^{\infty}$ denote the sequence of Fibonacci numbers, given as

$$(4.1) \quad F_0 = 0, \quad F_1 = 1, \quad F_{n+1} = F_n + F_{n-1}, \quad n \geq 1.$$

Proposition 4.2. For every $n \geq 0$,

$$(4.2) \quad O_{n+1} = 2O_n + A_n, \quad A_{n+1} = O_n + A_n$$

and

$$(4.3) \quad O_n = 10F_{2n+1}, \quad A_n = 10F_{2n}.$$

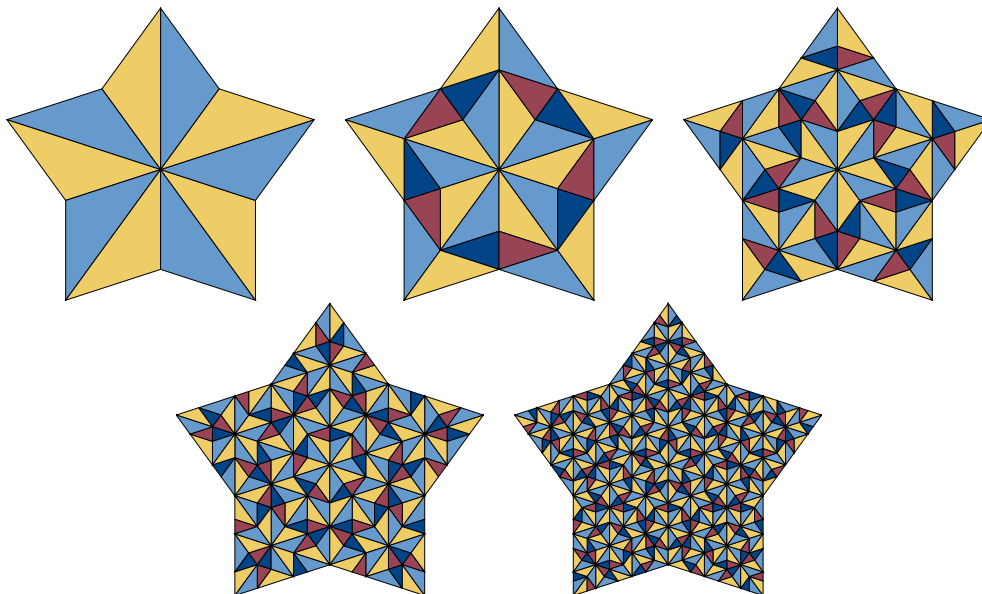


FIGURE 6. The first five levels of the tiling generated by the triangular substitution rule: $\mathcal{T}_0^{\blacktriangle}, \mathcal{T}_1^{\blacktriangle}, \dots, \mathcal{T}_4^{\blacktriangle}$.

The total number of tiles at level n is then

$$(4.4) \quad O_n + A_n = 10F_{2n+2}.$$

Proof. The recursion (4.2) follows immediately from the substitutions in Definition 2.4. One can check that (4.3) holds for $n = 0$ and $n = 1$ by inspection. Assuming it holds for all $k \leq n$ with $n \geq 1$ (4.2) yields

$$O_{n+1} = 2O_n + A_n = 10(2F_{2n+1} + F_{2n}) = 10F_{2n+3},$$

where we have applied the recursion of (4.1) twice in the final step. Similarly,

$$A_{n+1} = O_n + A_n = 10(F_{2n+1} + F_{2n}) = 10F_{2n+2},$$

which proves (4.3) by induction. Combining (4.3) and (4.1) gives (4.4). \square

4.2. Ring Modes.

Proposition 4.3. *Let Γ denote the graph associated with the polygonal tiling shown in Figure 7 and let Δ denote the corresponding Laplace operator. Define a vector ψ by*

$$(4.5) \quad \psi(T) = \begin{cases} 1, & T \text{ is blue;} \\ -1, & T \text{ is red;} \\ 0, & \text{otherwise.} \end{cases}$$

Then $\Delta\psi = 2\psi$.

Proof. The proof follows from a direct calculation. \square

Let \mathcal{R} denote the 20-tile pattern corresponding to the ring mode.

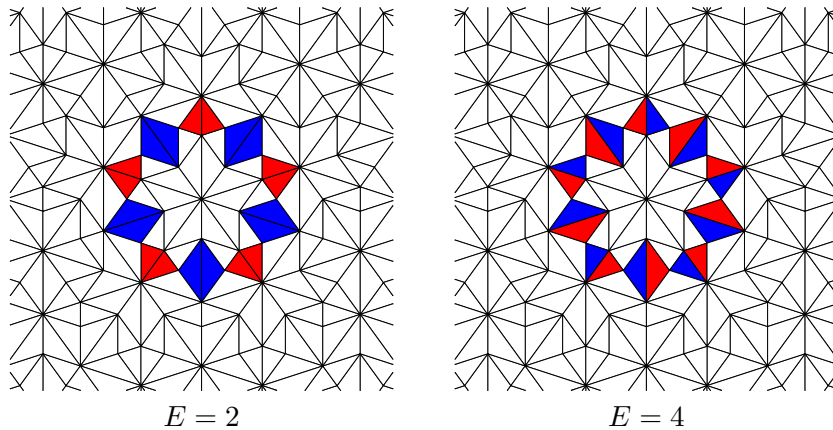


FIGURE 7. Locally-supported eigenfunctions for the Robinson triangle substitution, with $E = 2$ and $E = 4$. The nonzero entries of these modes take the values $+1$ (blue) and -1 (red).

Proposition 4.4. *Let $n \geq 5$ be given. The total number of occurrences of \mathcal{R} in \mathcal{T}_n is bounded from below by*

$$(4.6) \quad M_n = \sum_{\lfloor \frac{n-5}{2} \rfloor \geq k \geq 0} O_{n-5-2k} + \frac{1}{2} A_{n-5-2k}$$

The overall approach is similar to the corresponding calculation for the boat-star tiling, but the combinatorics are more complicated since the supports of the eigenfunctions may overlap with multiple supertiles.

Proof of Theorem 1.5. With the help of Propositions 4.2, 4.3, and 4.4, we get

$$\begin{aligned} k_{\blacktriangle}(2+) - k_{\blacktriangle}(2-) &\geq \lim_{n \rightarrow \infty} \frac{(O_{n-5} + O_{n-7} + \cdots) + \frac{1}{2}(A_{n-5} + A_{n-7} + \cdots)}{O_n + A_n} \\ &= \lim_{n \rightarrow \infty} \frac{(F_{2n-9} + F_{2n-13} + \cdots) + \frac{1}{2}(F_{2n-10} + F_{2n-14} + \cdots)}{F_{2n+2}} \\ &= \left(\varphi^{-11} + \frac{1}{2} \varphi^{-12} \right) (1 - \varphi^{-4})^{-1} \\ &= \frac{65 - 29\sqrt{5}}{20}, \end{aligned}$$

as desired. Since the same patterns produce the eigenfunctions at energy $E = 4$, the same argument works for that energy as well. \square

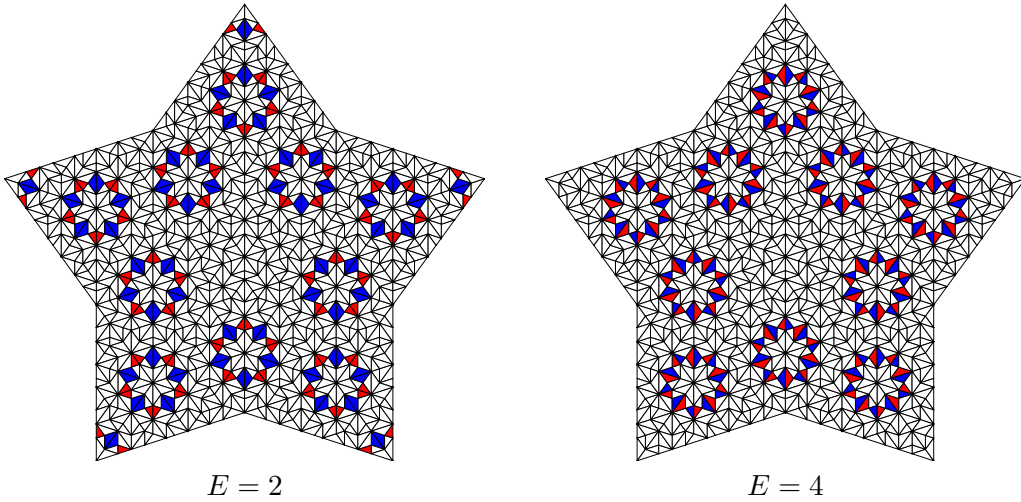


FIGURE 8. Localized modes for level 5 of the Robinson triangle substitution: for both eigenvalues there are ten “ring modes,” each supported on 20 tiles; for $E = 2$, five additional modes, each supported on four tiles, are made possible by the boundary.

TABLE 9. Robinson triangle tiling: the level of the tiling, the number of tiles, the multiplicity of $E = 2$, the multiplicity of $E = 4$, the number of boundary eigenfunctions for $E = 2$, and the jump in the approximant of the IDS at $E = 4$. The theoretically obtained lower bound from Theorem 1.5 is $(65 - 29\sqrt{5})/20 \approx 0.007701432625$.

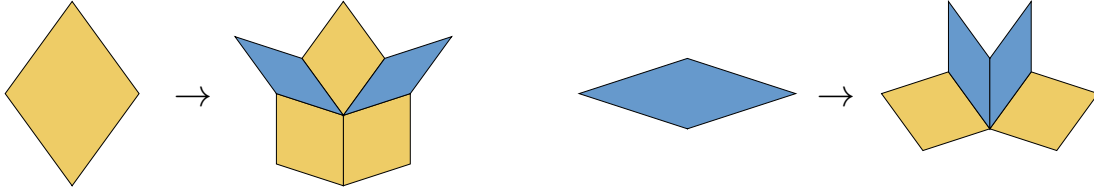
<i>level</i>	<i>tiles</i>	$E = 2$	$E = 4$	<i>boundary</i>	$k_{\blacktriangle,n}(4+) - k_{\blacktriangle,n}(4-)$
1	30	0	1	0	0.03333333...
2	80	1	1	0	0.01250000...
3	210	5	0	5	0.00000000...
4	550	6	1	5	0.00181818...
5	1 440	15	10	5	0.00694444...
6	3 770	36	21	15	0.00557029...
7	9 870	90	65	25	0.00658561...
8	25 840	216	181	35	0.00700464...
9	67 650	550	495	55	0.00731707...
10	177 110	1 411	1 316	95	0.00743041...
11	463 680	3 650	3 495	155	0.00753752...
12	1 213 930	9 471	9 226	245	0.00760010...
13	3 178 110	24 675	24 280	395	0.00763976...
14	8 320 400	64 401	63 756	645	0.00766261...
15	21 783 090	168 285	167 240	1 045	0.00767751...
16	57 028 870	440 046	438 361	1 685	0.00768665...
17	149 303 520	1 151 215	1 148 490	2 725	0.00769231...
18	390 881 690	3 012 556	3 008 141	4 415	0.00769578...

Figure 8 shows the locally-supported eigenfunctions at $E = 2$ and $E = 4$ for the level 5 tiling. Each of these energies correspond to ten ring modes; however, $E = 2$ has greater multiplicity as an eigenvalue of Δ_5 because of boundary modes supported on four tiles. The discrepancy of multiplicities between $E = 2$ and $E = 4$ grows at additional levels, as evident in the numerical calculations presented in Table 9. The convergence of the jump in the IDS at $E = 2$ and $E = 4$ is painfully slow. The largest tiling for which we have data contains 390,881,690 tiles, yet the IDS jump at $E = 4$ only agrees with the theoretically computed lower bound to about four decimal places.

5. RHOMBI

Definition 5.1. The *rhombus* substitution¹ is given by

¹Illustration following <https://tilings.math.uni-bielefeld.de/substitution/penrose-rhomb/>



In keeping with the star-shaped patterns generated by Definitions 2.4 and 3.1, we proceed as in Figure 10, alternating between applications of the substitution rule and trimming to a star shape. We obtain the eigenfunctions in Figures 11, 12, and 13, and numerically compute the values in Table 14.

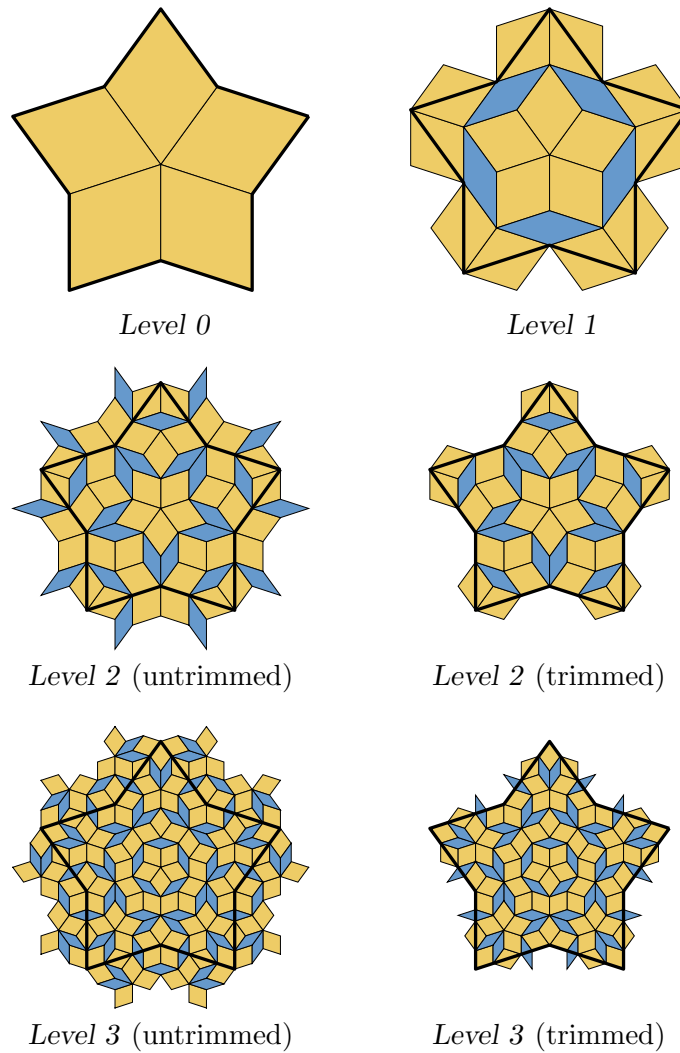


FIGURE 10. Rhombus rules applied to five rhombi at level 0, trimming to the original star shape at each iteration.

In contrast with the locally-supported eigenfunctions identified for the boat–star and Robinson triangle cases in the last two sections, for the rhombus tiling a variety of distinct locally-supported eigenfunction configurations with overlapping local support emerge at low levels, associated with energy $E = 6$. Figure 11 shows four such mode shapes at level 5. The eigenfunctions take values $+1$ on blue tiles and -1 on red tiles (with intermediate values indicated by a difference in shading) and are zero on the uncolored tiles. We classify these mode shapes as:

- *filled circle*, supported on 25 tiles;
- *big star*, supported on 50 tiles;
- *two star*, supported on 15 tiles;
- *diamond ring*, supported on 18 tiles.

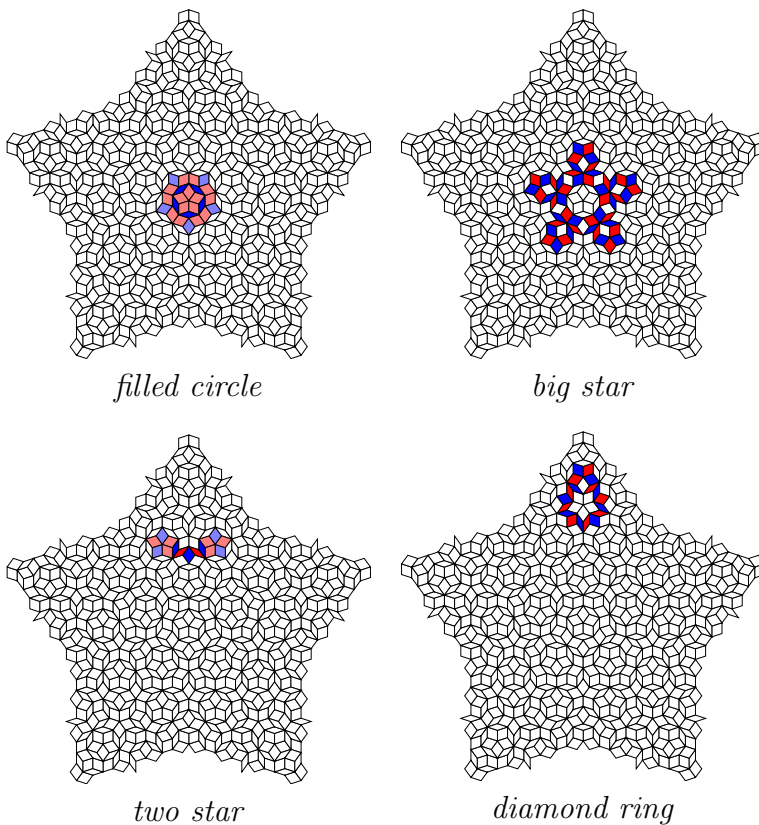


FIGURE 11. For the rhombus tiling, four linearly independent eigenfunctions at energy $E = 6$ at level 5. We refer to these configurations as the *filled circle*, *big star*, *two star*, and *diamond ring*. (Dark blue and dark red correspond to values ± 1 ; light blue and light red correspond to $\pm 1/2$.) Level 5 exhibits 1 filled circle mode, 1 big star mode, 10 diamond ring modes, and 15 two star modes, giving a total of 27 linearly independent eigenfunctions.

Locally-supported eigenfunctions of the Laplacian on the rhombus tiling have been studied before, notably by Fujiwara, Arai, Tokihiro, and Kohmoto in [9]. (It bears mentioning that Equation (2.1) in [9] differs from our Equation (2.1) in the first term, so energy $E = 2$ in [9] corresponds to $E = 6$ in Table 14.) Indeed, Fujiwara et al. describe five eigenfunctions named A1, A2, B, C, and D, and find a cumulative frequency of 0.068189. In Figure 11, we refer to their B state as a *two star* mode, and their D state as a *diamond ring* mode. Figure 12 shows instances where the modes A1, A2, and C can be constructed as linear combinations of the primitive mode shapes in Figure 11. The construction of C reveals a subtlety that complicates the counting of linearly independent modes: in some cases a *diamond ring* mode can be realized as the combination of a different *diamond ring* and a *two star* mode.

The rhombus tiling exhibits another intriguing property: the emergence of more complicated locally-supported modes on larger tilings. At level 6 the eigenvalue $E = 6$ has multiplicity 102. One can identify 10 filled circle modes, 10 big star modes, 20 diamond ring modes, and 60 two star modes, accounting for 100 linearly independent eigenfunctions. One can then find two additional linearly independent eigenfunctions, still having local support away from the boundary, but now involving many more tiles. Figure 13 shows these two modes, one supported on 200 tiles, the other on 245 tiles. (It does not appear that the modes in Figure 13 were identified

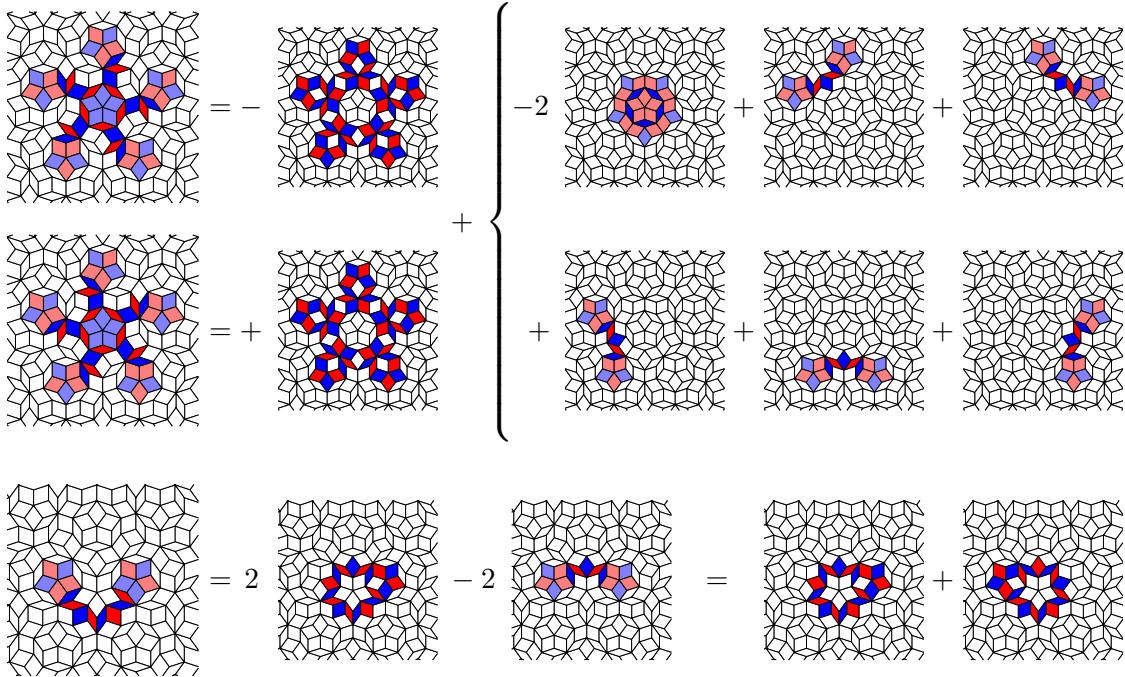


FIGURE 12. Construction of eigenfunctions A1, A2, and C of Fujiwara–Arai–Rokihiko–Kohmoto [9] for the rhombus substitution as linear combinations of our basis of locally-supported eigenfunctions.

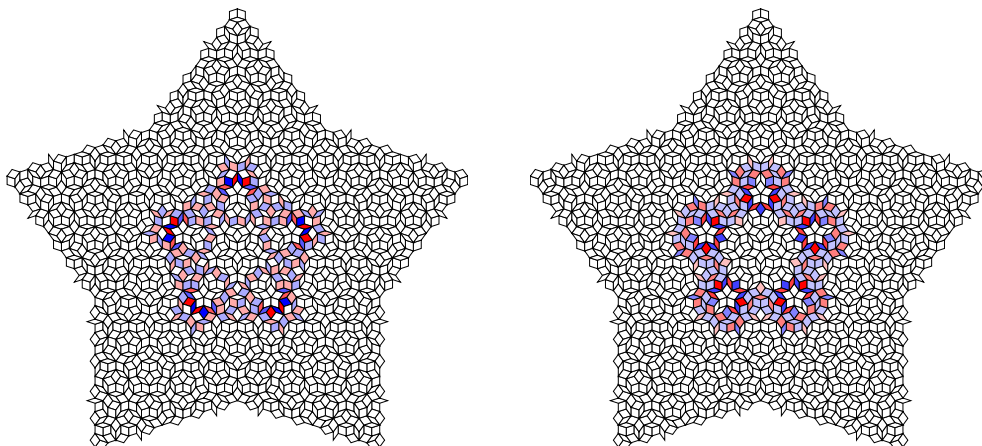


FIGURE 13. Two linearly independent eigenfunctions for $E = 6$ at level 6. Though locally supported, neither is a linear combination of the other 100 modes of the types shown in Figure 11. (The vector on the left is supported on 200 tiles, with nonzero entries ± 1 , $\pm 2/3$, and $\pm 1/3$; the vector on the right is supported on 245 tiles, with nonzero entries 1 , $\pm 3/4$, $\pm 1/2$, and $\pm 1/4$.)

TABLE 14. Rhombus tiling: the level of the tiling, the number of tiles, and the multiplicity of eigenvalue $E = 6$ at levels 1–14. The final column shows the numerical approximation to the IDS jump.

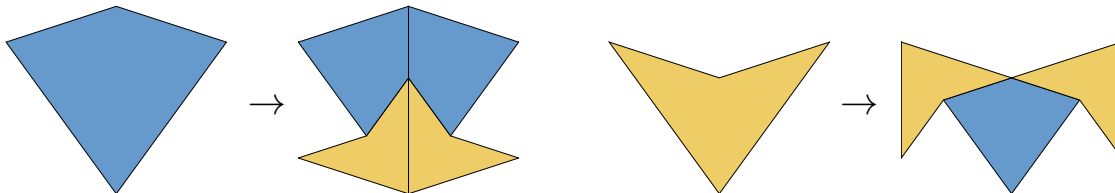
<i>level</i>	<i>tiles</i>	$E = 6$	$k_{\blacklozenge,n}(6+) - k_{\blacklozenge,n}(6-)$
1	20	0	0.00000000...
2	45	0	0.00000000...
3	115	2	0.01739130...
4	290	5	0.01724137...
5	745	27	0.03624161...
6	1 925	102	0.05298701...
7	5 000	287	0.05740000...
8	13 025	797	0.06119001...
9	33 995	2 164	0.06365642...
10	88 830	5 792	0.06520319...
11	232 285	15 409	0.06633661...
12	607 685	40 744	0.06704789...
13	1 590 220	107 289	0.06746802...
14	4 162 085	281 939	0.06773984...

in [9].) Like the simpler modes in Figure 11, these shapes must recur at higher levels; moreover, yet more sophisticated locally-supported modes could also manifest at higher levels. The emergence of such modes illustrates the challenge in explicitly

calculating the jump in the integrated density of states at $E = 6$; moreover, the rarity of such modes (in comparison with the more abundant mode shapes in Figure 11) indicates the challenge of precisely estimating this jump numerically. Table 14 shows numerical computations for this jump up through level 14 (4,162,085 tiles).

6. KITES AND DARTS

Definition 6.1. The *kite-dart* substitution² is given by



Analogous to the rhombus tiling, we start at level 0 with a star-shaped configuration (comprising five darts), and then alternate between applications of the substitution rule and trimming back to maintain the star-shaped pattern. Figure 16 shows the first four steps of this process.

In contrast to the previous examples, this tiling supports locally supported eigenfunctions supported away from the boundary at *irrational* energies. At level 5, such eigenfunctions emerge at $E = 6 - \varphi = 4.381966\dots$ and $E = 5 + \varphi = 6.618033\dots$ (In contrast to the other tilings we consider, this latter energy appears to be at the top of the spectrum.) These eigenfunctions can be represented as rings of 40 tiles

²Illustration following <https://tilings.math.uni-bielefeld.de/substitution/penrose-kite--dart/>

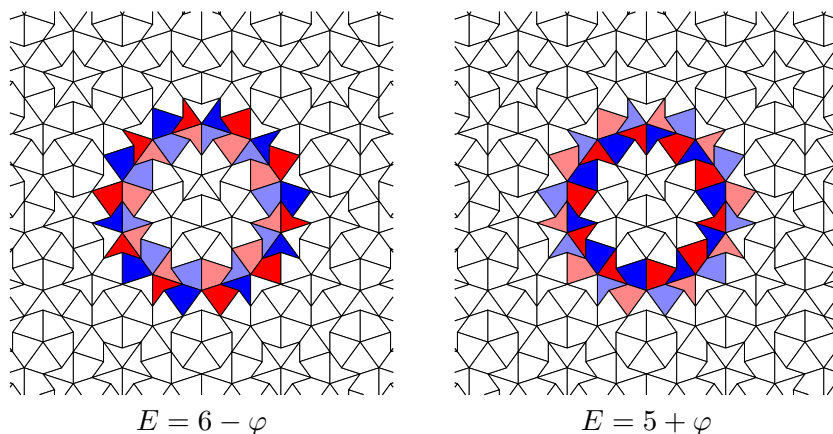


FIGURE 15. Locally-supported eigenfunctions for the kite-dart substitution, corresponding to $E = 6 - \varphi = 4.381966\dots$ and $E = 5 + \varphi = 6.618033\dots$. The nonzero entries of these ring modes take the values $+1$ (dark blue), $+1/\varphi$ (light blue), $-1/\varphi$ (light red), and -1 (dark red).

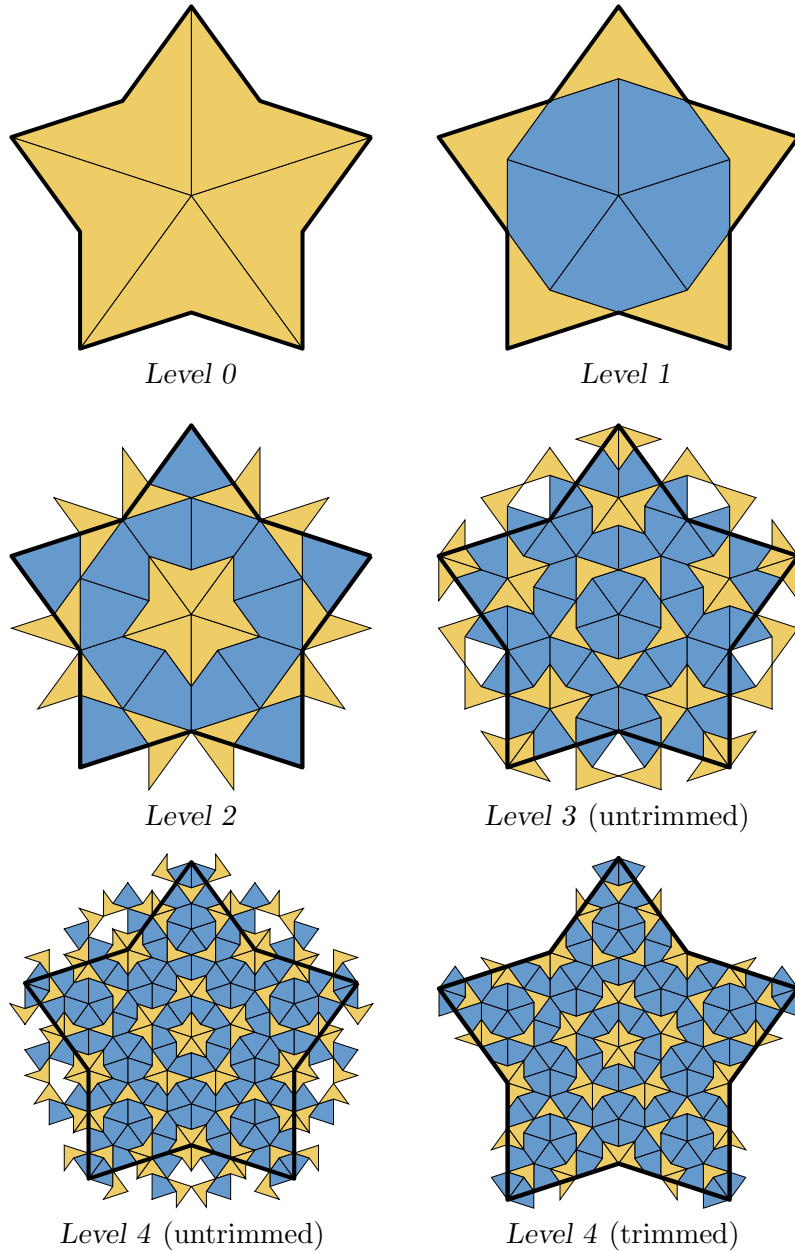


FIGURE 16. Kite–dart rules applied to a starting configuration of five darts at level 0.

(20 kites and 20 darts) taking the values ± 1 and $\pm 1/\varphi$, as illustrated in Figure 15. While these ring modes may superficially resemble those obtained for the Robinson triangle (see Figure 7), counting the frequency of these kite–dart modes is significantly complicated by their overlapping support. Figure 17 shows the sum of the five ring modes that emerge at level 5 at $E = 6 - \varphi$ and $E = 5 + \varphi$. (Contrast Figure 17 to the analogous illustration for the Robinson triangle tiling in Figure 8.)

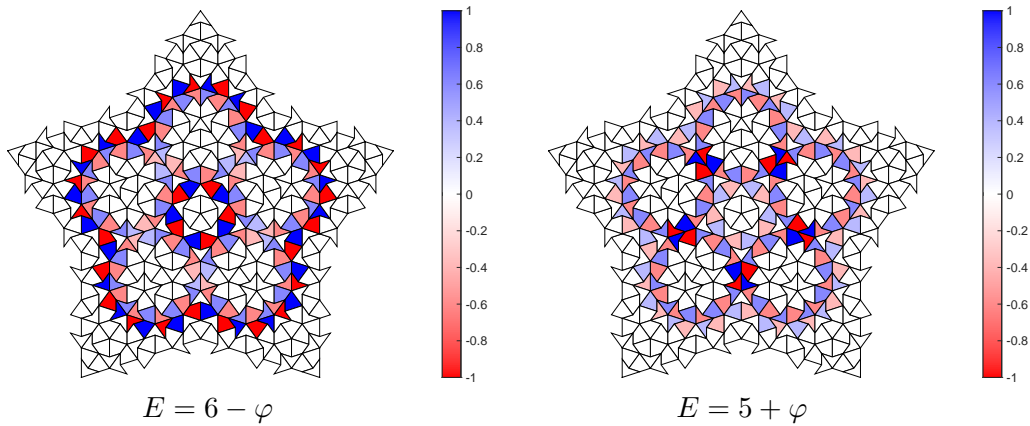


FIGURE 17. Sum of five “ring modes” for level 5 of the kite–dart substitution for $E = 6 - \varphi$ and $E = 5 + \varphi$, illustrating the overlapping support of these modes.

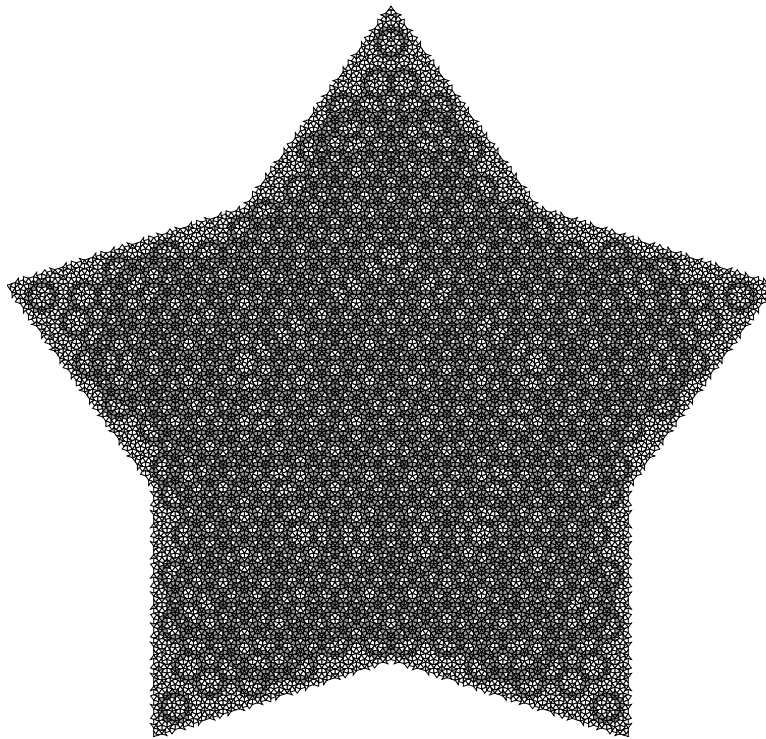


FIGURE 18. The gray tiles show the support of the eigenfunctions at $E = 5 + \varphi$ and $E = 6 - \varphi$ for the kite–dart tiling at level 9.

Figure 18 shows the support of the eigenfunctions for these two energies at level 9, each of which has multiplicity 435. The support covers 13,535 of the 21,025 tiles.

TABLE 19. Kite–dart tiling: The level of the tiling, the number of tiles, the multiplicities of $E = 5 + \varphi$ and $E = 6 - \varphi$, and the jump in the corresponding approximant of the IDS at each of these energies.

<i>level</i>	<i>tiles</i>	$E = 6 - \varphi$	$E = 5 + \varphi$	$k_{\clubsuit,n}(E_{\clubsuit+}) - k_{\spadesuit,n}(E_{\spadesuit+})$
1	10	0	0	0.00000000...
2	30	0	0	0.00000000...
3	75	0	0	0.00000000...
4	180	0	0	0.00000000...
5	460	5	5	0.01086956...
6	1 195	10	10	0.00836820...
7	3 100	50	50	0.01612903...
8	8 060	135	135	0.01674938...
9	21 025	435	435	0.02068965...
10	54 930	1 185	1 185	0.02157291...
11	143 610	3 305	3 305	0.02301371...
12	375 645	8 875	8 875	0.02362603...
13	982 930	23 735	23 735	0.02414719...
14	2 572 510	62 820	62 820	0.02441973...

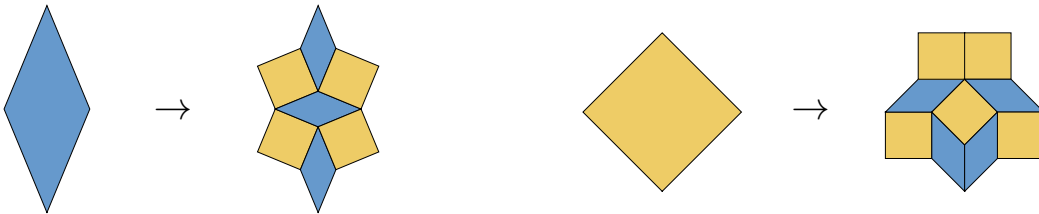
The complement of this support exhibits interesting patterns, including many “short bow ties” [10, 13].

Our numerical computations suggest that $E = 6 - \varphi$ and $E = 5 + \varphi$ have the same multiplicity (a multiple of 5) up through level 14 (2,572,510 tiles). Table 19 reports these frequencies, along with the jump each induces in the integrated density of states.

7. AMMANN–BEENKER

Thus far we have investigated four versions of the Penrose tiling. In this section we explore related questions for the Ammann–Beenker tiling. We begin by recalling the substitution rule.

Definition 7.1. The *Ammann–Beenker* substitution³ is given by



As in previous sections, we generate a tiling by beginning with an initial seed and iteratively applying the substitution rule. Let $\mathcal{T}_0^\blacksquare$ denote the pattern consisting of

³Illustration following <https://tilings.math.uni-bielefeld.de/substitution/ammann-beenker/>

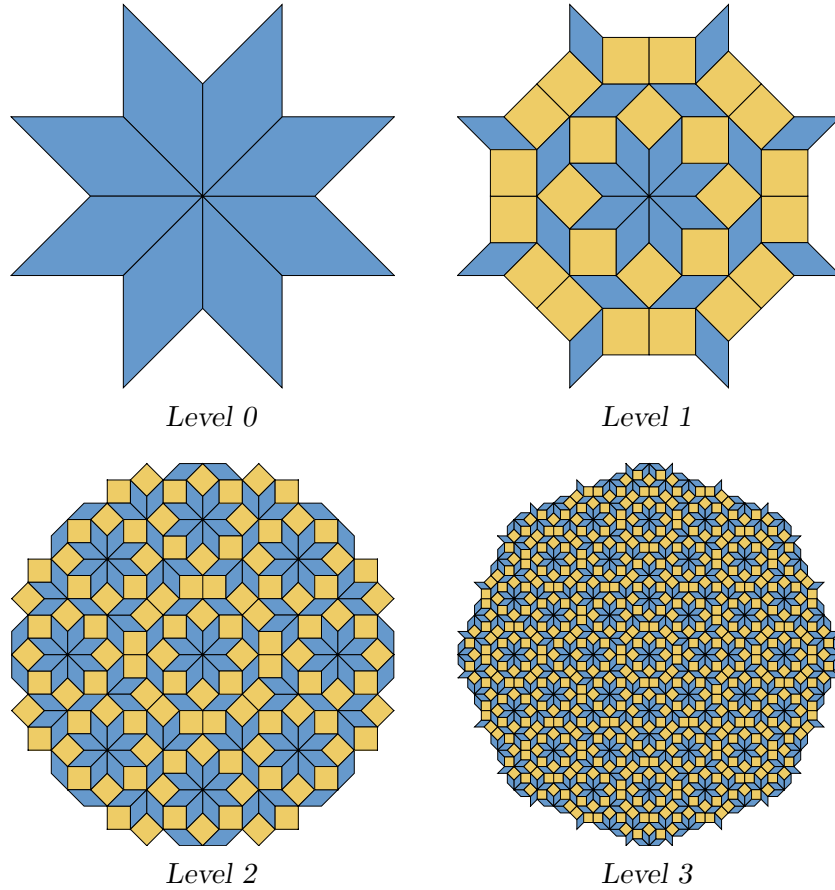


FIGURE 20. Three iterations of the Ammann–Beenker rules applied to an initial seed of eight thin rhombi: $\mathcal{T}_0^\blacksquare, \dots, \mathcal{T}_3^\blacksquare$.

eight thin rhombi arranged in an eight-point star shape as in Figure 20. Analogous to the kite–dart substitution (see Figure 16), we alternate between applications of the substitution rule and trimming back to an octagon. We let $\mathcal{T}_n^\blacksquare$ denote n steps of this process.

Theorem 7.2. *The Ammann–Beenker tiling has eigenfunctions at energies $E_\blacksquare = 4, 6$. Denoting $\lambda = \sqrt{2} - 1$, we have*

$$\begin{aligned} k_\blacksquare(4+) - k_\blacksquare(4-) &\geq \lambda^4 + \lambda^6 + 2\lambda^8 = 1270 - 898\sqrt{2} = 0.0362209\dots, \\ k_\blacksquare(6+) - k_\blacksquare(6-) &\geq \lambda^4 + \lambda^6 = 116 - 82\sqrt{2} = 0.0344878\dots \end{aligned}$$

Proof. As can be seen from Figures 20, 21, 22, and 24, each occurrence of the eight-fold vertex star produces an eigenfunction at both energies, each once-substituted version also gives an eigenfunction at both energies, and each twice-substituted vertex star produces an additional pair of eigenfunctions at energy $E = 4$. One can check visually that the support of each eigenfunction is not contained in the union

of the supports of the other eigenfunctions, and hence each occurrence of each patch contributes a linearly independent vector to the corresponding eigenspace.

Thus, the estimates contain three pieces that correspond to the frequencies of the eightfold vertex star, and the result of substituting it once and twice. The frequency of the eight-fold star is λ^4 , as computed in [2]. The frequencies of the other patches can be seen to be bounded from below by $\lambda^2 \cdot \lambda^4 = \lambda^6$ (for the once-substituted eightfold vertex star) and $\lambda^4 \cdot \lambda^4 = \lambda^8$ (for the twice-substituted version), which can be seen by the multi-dimensional analog of the relevant material in Sections 5.3 and 5.4 of [28]. To work out this analog, one needs to invoke uniform existence results for the limits defining the frequencies in question, which are contained, for example, in [6] and [11]. \square

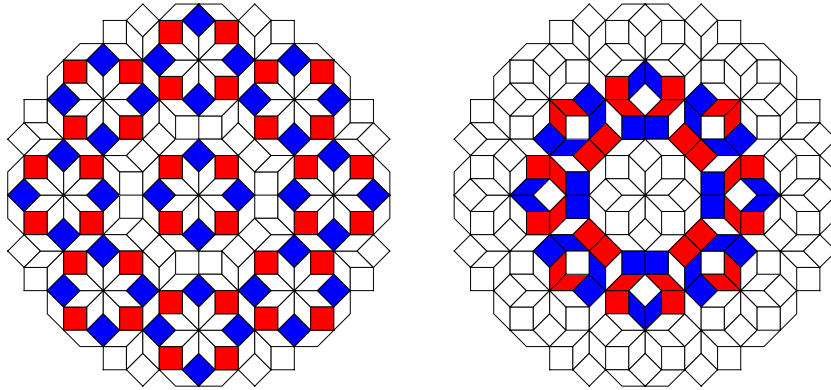


FIGURE 21. Ten linearly independent eigenfunctions at energy $E = 4$ (nine on the left, each supported on 8 tiles; one on the right, supported on 64 tiles) at level 2.

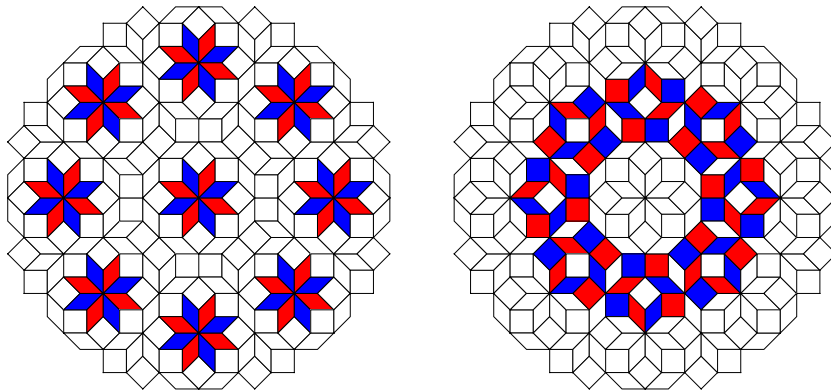


FIGURE 22. Ten linearly independent eigenfunctions at energy $E = 6$ (nine on the left, each supported on 8 tiles; one on the right, supported on 64 tiles) at level 2.

TABLE 23. Ammann–Beenker tiling: The level of tiling, number of tiles, multiplicities of eigenvalues $E = 4$ and $E = 6$, and the jump in the IDS at $E = 6$.

<i>level</i>	<i>tiles</i>	$E = 4$	$E = 6$	$k_{\blacksquare,n}(4+) - k_{\blacksquare,n}(4-)$	$k_{\blacksquare,n}(6+) - k_{\blacksquare,n}(6-)$
1	48	3	1	0.062500...	0.020833...
2	256	11	11	0.042969...	0.042969...
3	1 392	44	42	0.031609...	0.030172...
4	7 984	276	258	0.034726...	0.032315...
5	46 160	1 604	1 538	0.034749...	0.033319...
6	268 256	9 556	9 106	0.035622...	0.033945...
7	1 561 552	56 116	53 490	0.036256...	0.034254...
8	9 096 784	328 420	312 834	0.036102...	0.034389...

In Figures 21 and 22 we present ten locally-supported eigenfunctions that correspond to energies $E = 4$ and $E = 6$, respectively. Table 23 reports the numerically computed multiplicities of these eigenvalues up through level 8 (9,096,784 tiles). An observant reader may notice that the level 2 row of Table 23 indicates the existence of an eleventh eigenfunction not shown in Figures 21 and 22. This extra mode lies on the boundary and thus is an artifact of the finite-volume truncation.

Theorem 7.2 gives different lower bounds on the jump in the integrated density of states for $E = 4$ and $E = 6$. The discrepancy in the multiplicity of these eigenvalues emerges at level 3, where $E = 4$ admits two additional eigenfunctions that are not in the span of the simple mode shapes in Figure 21. While still locally supported, these two modes involve many more tiles: the eigenfunctions in Figure 24, supported on 104 tiles and 328 tiles, provide a basis for this extra two-dimensional eigenspace.

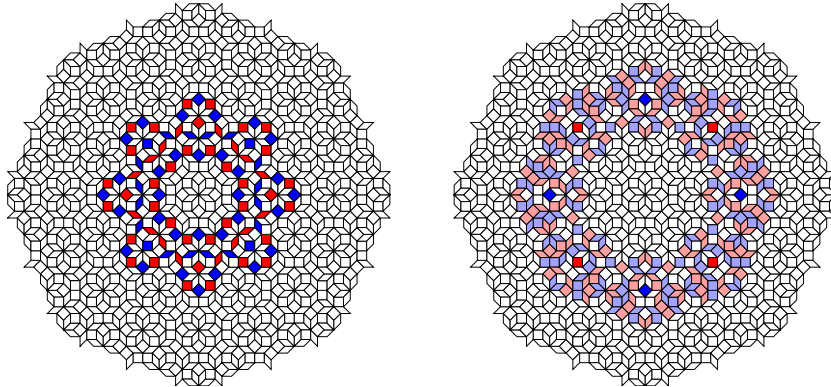


FIGURE 24. Two locally-supported eigenfunctions at level 3 for energy $E = 4$ that did not appear on lower levels of the substitution; the one on the left is supported on 104 tiles with nonzero values ± 1 ; the one on the right is supported on 328 tiles with nonzero values ± 1 and $\pm 1/2$.

Accounting for the recurrence of such mode shapes at higher levels explains the discrepancy of the bounds for $E = 4$ and $E = 6$ in Theorem 7.2. The situation is analogous to the rhombus tiling, where apparently new mode shapes emerged at higher levels (see Figure 13). Whether modes with additional complexity emerge at still higher levels is an open question; the presence of such modes is difficult to tease out from numerical approximations to the jump in the integrated density of states, given the relative rarity of those modes and the additional complication of modes supported on the boundary.

8. QUESTIONS AND OPEN PROBLEMS

Let us conclude by showing numerically-computed approximations to the integrated density of states (IDS) for the five tilings we have discussed, and posing some questions these plots suggest. On one hand, the IDS is a fundamental spectral quantity. On the other hand, the shape of the graph of the IDS naturally suggests several possibilities. Concretely:

- (1) A sharp vertical jump suggests the presence of an eigenvalue corresponding to an eigenfunction. Indeed, this is precisely how many of the examples from the present work were observed. Of course, one must be careful here, since one is looking at eigenvalue counting functions associated to finite tilings, so *every* jump is sharp. A simple eigenvalue causes a jump of size $1/(\# \text{ tiles})$; higher multiplicities give bigger jumps. One is looking for a jump that is stable, i.e., the size of the jump stays bounded from below as the level of the tiling is increased.
- (2) Since the IDS is constant on each connected component of the complement of the spectrum, a flat section in the plot of the approximations of the IDS that is stable upon iterating the substitution rule suggests the presence of a spectral gap.
- (3) Conversely, the spectrum is given by the set of points of increase of the IDS, so an interval on which the IDS is everywhere increasing corresponds to an interval that is completely contained in the spectrum.

Figure 25 shows several finite-patch approximations to the IDS associated with the boat–star tiling. To produce this plot (and the other IDS plots that follow), we prefer to compute all eigenvalues of Δ_n numerically (using `eig` in MATLAB). While expensive, this calculation allows one to evaluate the multiplicity of eigenvalues (subject to rounding errors that are well understood for symmetric eigenvalue calculations). In Figure 25, this `eig` approach is feasible up through level 5 (30,406 tiles). For level 6 (210,181 tiles) and level 7 (1,447,691 tiles), we use a different strategy inspired by spectrum slicing [26, sect. 3.3]). The spectral interval is finely discretized with points $\{E_j\}$. For each E_j , we use MATLAB’s `ldl` command to compute a factorization $L - E_j = L_j D_j L_j^T$, where L_j is a permuted unit lower-triangular matrix and D_j is block-diagonal, having 1-by-1 and 2-by-2 diagonal blocks [12, sect. 4.4]. By Sylvester’s Law of Inertia, the congruent matrices $L - E_j$ and D_j have the same number of negative eigenvalues; the block diagonal form of

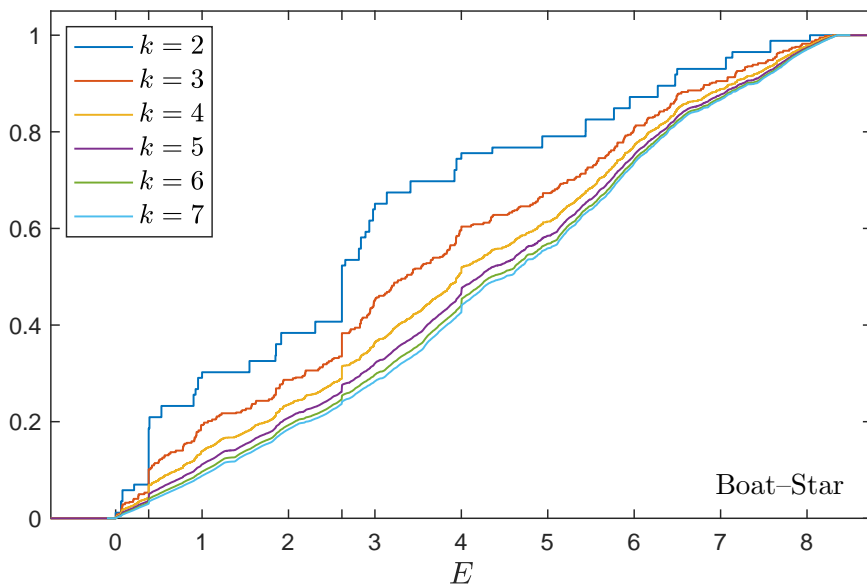


FIGURE 25. Computed integrated density of states for the boat–star tiling, levels 2 through 7. Notice the (diminishing) jumps at $1/\varphi^2 \approx 0.381966$ and $\varphi^2 \approx 2.618034$ due to the boundary modes shown in Figure 5; the jump at $E = 4$ is due to ring modes of the form shown in Figure 2.

D_j makes that number easy to count. Since the negative eigenvalues of $L - E_j$ reveal the number of eigenvalues of L smaller than E_j , these counts collectively give an approximation to the IDS. (Indeed, we also use this approach to count the multiplicity of special energies known to have locally-supported eigenfunctions, as presented in the tables throughout this paper. For these counts, we take slices just above and below the target energy; in most cases we vary the slice size to gain confidence in the presented numbers.)

One observes some interesting features that prompt the following questions. First, one is interested in the topological structure of the spectrum.

Question 8.1. Let Σ_\star denote the spectrum associated with the boat–star tiling. Is the interior of Σ_\star nonempty? If the interior is nonempty, is it dense in Σ_\star ?

We expect that establishing the presence, let alone density, of intervals in the spectrum to be quite challenging. The plots of the approximants to the IDS suggest that one may start looking for nonempty intervals near the extrema of the spectrum. Thus, we pose separately the following question, which may be approachable via perturbative methods.

Question 8.2. Does there exist $\delta > 0$ such that

$$(8.1) \quad [0, \delta) \cup (\max \Sigma_\star - \delta, \max \Sigma_\star] \subseteq \Sigma_\star?$$

The estimation and computation of extrema of the spectrum is a separately interesting question. The bottom is given by $E = 0$ by elementary arguments, but the top of the spectrum is not always trivial to compute, so we also ask:

Question 8.3. Can one compute $\max \Sigma_\star$ in closed form?

It is clear from [15] that one may “insert” a locally-supported eigenfunction into a Laplacian on any MLD class. Namely, the MLD class of any tiling contains a tiling whose nearest neighbor Laplacian has locally-supported eigenfunctions.

Question 8.4. Can one always remove a locally-supported eigenfunction from a Laplacian on any MLD class? Is it even true that for every MLD class, there exists a tiling in that class whose associated Laplacian does not have any locally-supported eigenfunctions?

On the one hand, as we just mentioned, one can always ensure the presence of some locally supported eigenfunction for a suitable choice of tiling in an MLD class, and then, assuming the model in question is linearly repetitive, this will always lead to a jump in the IDS. On the other hand, as we have seen in this paper, the IDS may in fact have multiple jumps in some cases. This naturally leads to the following question.

Question 8.5. Is the number of jumps in the IDS always finite? Is there an effective way of bounding this number for a given linearly repetitive tiling?

Note that if the previous question has an affirmative answer, the IDS will be piecewise continuous, and then it is natural to ask for stronger regularity properties

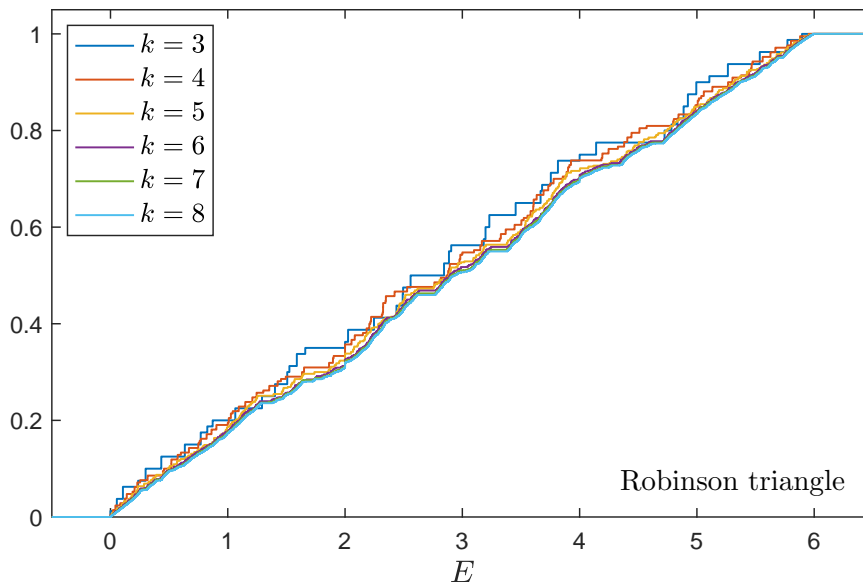


FIGURE 26. Computed integrated density of states for the Robinson triangle tiling, levels 3 through 8. Note the jumps at $E = 2$ and $E = 4$.

on these pieces. Specifically, based on the shape of the IDS plots we have exhibited, we ask the following:

Question 8.6. Near the top or bottom of the spectrum, is the IDS α -Hölder continuous? Lipschitz continuous?

Figure 26 shows several finite-patch approximations to the IDS associated with the Robinson triangle tiling. The reader can observe the jumps at energies $E = 2$ and $E = 4$. As mentioned before, the spectrum is given by the set of points of increase of the IDS. As such, the parts of this IDS plot that correspond to the bottom and top of the spectrum are somewhat suggestive.

Question 8.7. Investigate the analogs of Questions 8.1, 8.2, and 8.6 for the Robinson triangle tiling.

Notice an intriguing feature of the graph of the approximants to the IDS of the Robinson tiling in Figure 26: the emergence of what appear to be relatively stable spectral gaps (e.g., a bit to the left and right of $E = 3$). Figure 27 examines this possibility in finer detail: we compare finitely computed eigenvalues of Δ_n as n grows, looking for persistent gaps. Beyond the level at which we can compute all eigenvalues of Δ_n , we use spectrum slicing to locate eigenvalues that define the edge of the intervals that were suggested at lower levels. Figure 27 shows six such gaps

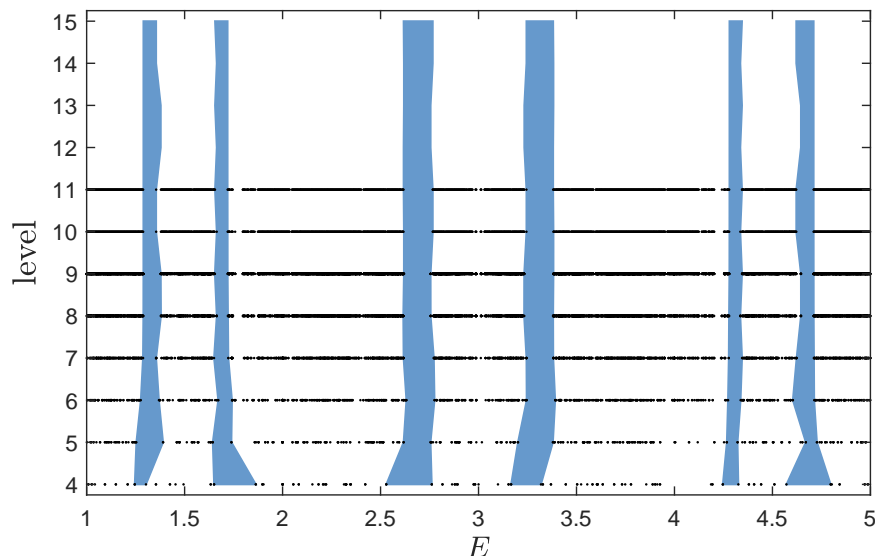


FIGURE 27. The spectra of finite-patch approximations of the Robinson triangle tiling exhibit gaps that apparently persist as the level is increased, corresponding to plateaus in the integrated density of states. This image shows numerically computed interior bounds for six gaps (blue regions) as the level k increases. For lower levels, we also show all computed eigenvalues as black dots. Several additional gaps are apparent. (We suspect there are infinitely many such gaps.)

in blue; several other potential gaps (e.g., to the right of the second blue gap, near $E = 3$, and to the left of the fifth blue gap) are also apparent. It would be interesting to verify this phenomenon rigorously.

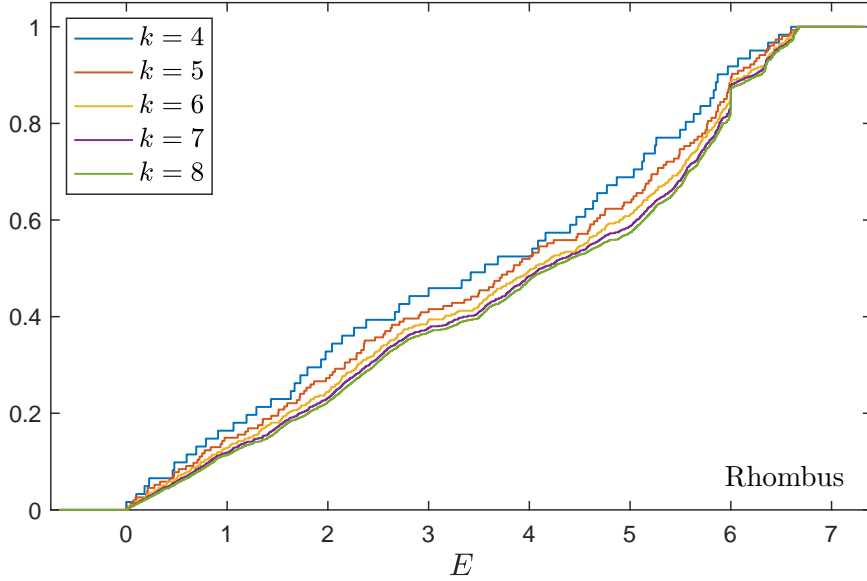


FIGURE 28. Computed integrated density of states for the rhombus tiling, levels 4 through 8. Note the jump at $E = 6$.

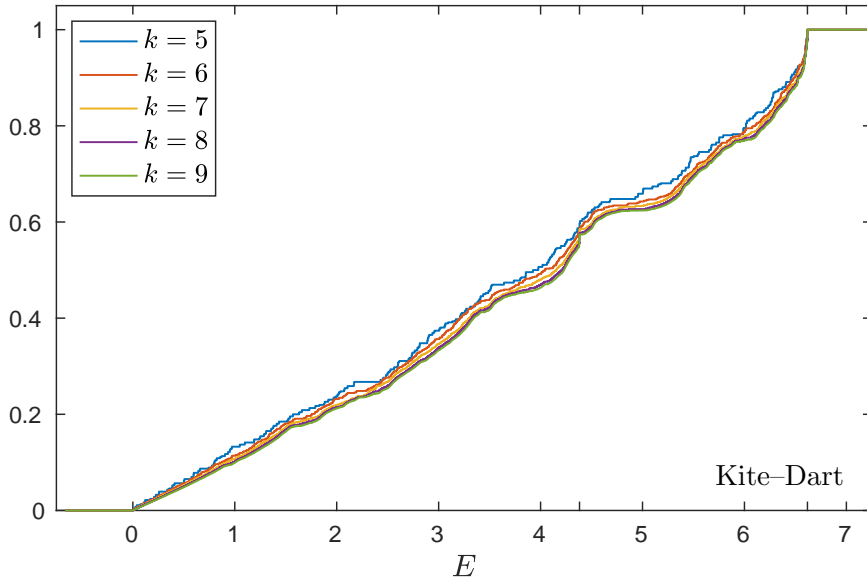


FIGURE 29. Computed integrated density of states for the kite-dart tiling, levels 5 through 9. Note the jumps at $E = 6 - \varphi = 4.381966\dots$ and $E = 5 + \varphi = 6.618033\dots$ (at the top of the spectrum).

Question 8.8. Show that Σ_{\blacktriangle} has a nontrivial spectral gap. Are there infinitely many?

We conclude with approximations to the IDS for the rhombus, kite–dart, and Ammann–Beenker tilings in Figures 28, 29, and 30. These plots have similar features to the first two, and hence one may ask similar questions to Questions 8.1–8.8.

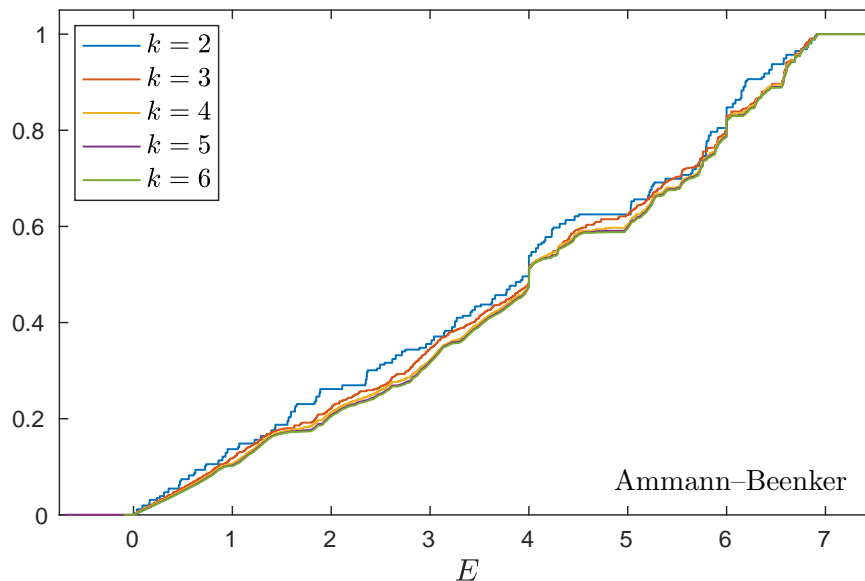


FIGURE 30. Computed integrated density of states for the Ammann–Beenker tiling, levels 2 through 6. Note the jumps at $E = 4$ and $E = 6$.

REFERENCES

- [1] M. Arai, T. Tokihiro, T. Fujiwara, and M. Kohmoto. Strictly localized states on a two-dimensional Penrose lattice. *Phys. Rev. B* (3), 38(3):1621–1626, 1988.
- [2] M. Baake and U. Grimm. *Aperiodic order. Vol. 1*, volume 149 of *Encyclopedia of Mathematics and its Applications*. Cambridge University Press, Cambridge, 2013. A mathematical invitation, With a foreword by Roger Penrose.
- [3] M. Baake and U. Grimm. *Aperiodic order. Vol. 2*, volume 166 of *Encyclopedia of Mathematics and its Applications*. Cambridge University Press, Cambridge, 2017.
- [4] M. Baake and R. V. Moody, editors. *Directions in mathematical quasicrystals*, volume 13 of *CRM Monograph Series*. American Mathematical Society, Providence, RI, 2000.
- [5] D. Damanik, A. Gorodetski, and W. Yessen. The Fibonacci Hamiltonian. *Invent. Math.*, 206(3):629–692, 2016.
- [6] D. Damanik and D. Lenz. Linear repetitivity. I. Uniform subadditive ergodic theorems and applications. *Discrete Comput. Geom.*, 26(3):411–428, 2001.
- [7] N. P. Frank. A primer of substitution tilings of the Euclidean plane. *Expo. Math.*, 26(4):295–326, 2008.
- [8] D. Frettlöh, E. Harriss, and F. Gähler. Tilings encyclopedia. <https://tilings.math.uni-bielefeld.de>.

- [9] T. Fujiwara, M. Arai, T. Tokihiro, and M. Kohmoto. Localized states and self-similar states of electrons on a two-dimensional Penrose lattice. *Phys. Rev. B (3)*, 37(6):2797–2804, 1988.
- [10] M. Gardner. *Penrose Tiles to Trapdoor Ciphers*. Mathematical Association of America, Washington, DC, revised edition, 1997.
- [11] C. P. M. Geerse and A. Hof. Lattice gas models on self-similar aperiodic tilings. *Rev. Math. Phys.*, 3(2):163–221, 1991.
- [12] G. H. Golub and C. F. Van Loan. *Matrix Computations*. Johns Hopkins University Press, Baltimore, fourth edition, 2012.
- [13] B. Grünbaum and G. C. Shephard. *Tilings and Patterns*. W. H. Freeman and Company, New York, 1987.
- [14] J. Kellendonk, D. Lenz, and J. Savinien, editors. *Mathematics of aperiodic order*, volume 309 of *Progress in Mathematics*. Birkhäuser/Springer, Basel, 2015.
- [15] S. Klassert, D. Lenz, and P. Stollmann. Discontinuities of the integrated density of states for random operators on Delone sets. *Comm. Math. Phys.*, 241(2-3):235–243, 2003.
- [16] M. Kohmoto and B. Sutherland. Electronic states on a Penrose lattice. *Phys. Rev. Lett.*, 56:2740–2743, 1986.
- [17] M. Kohmoto, B. Sutherland, and C. Tang. Critical wave functions and a Cantor-set spectrum of a one-dimensional quasicrystal model. *Phys. Rev. B (3)*, 35(3):1020–1033, 1987.
- [18] D. Lenz and P. Stollmann. Algebras of random operators associated to Delone dynamical systems. *Math. Phys. Anal. Geom.*, 6(3):269–290, 2003.
- [19] D. Lenz and P. Stollmann. Delone dynamical systems and associated random operators. In *Operator algebras and mathematical physics (Constanța, 2001)*, pages 267–285. Theta, Bucharest, 2003.
- [20] D. Lenz and P. Stollmann. An ergodic theorem for Delone dynamical systems and existence of the integrated density of states. *J. Anal. Math.*, 97:1–24, 2005.
- [21] M. Mirzhalilov and M. Ö. Oktel. Perpendicular space accounting of localized states in a quasicrystal. *Phys. Rev. B*, 102, 2020.
- [22] R. V. Moody, editor. *The mathematics of long-range aperiodic order*, volume 489 of *NATO Advanced Science Institutes Series C: Mathematical and Physical Sciences*. Kluwer Academic Publishers Group, Dordrecht, 1997.
- [23] M. Ö. Oktel. Strictly localized states in the octagonal Ammann-Beenker quasicrystal. *Phys. Rev. B*, 104, 2021.
- [24] M. Ö. Oktel. Localized states in local isomorphism classes of pentagonal quasicrystals. preprint: arXiv:2203.09899, 2022.
- [25] S. Ostlund, R. Pandit, D. Rand, H. J. Schellnhuber, and E. D. Siggia. One-dimensional Schrödinger equation with an almost periodic potential. *Phys. Rev. Lett.*, 50(23):1873–1876, 1983.
- [26] B. N. Parlett. *The Symmetric Eigenvalue Problem*. SIAM, Philadelphia, SIAM Classics edition, 1998.
- [27] J. Patera, editor. *Quasicrystals and discrete geometry*, volume 10 of *Fields Institute Monographs*. American Mathematical Society, Providence, RI, 1998.
- [28] M. Queffélec. *Substitution dynamical systems—spectral analysis*, volume 1294 of *Lecture Notes in Mathematics*. Springer-Verlag, Berlin, second edition, 2010.
- [29] D. Shechtman, I. Blech, D. Gratias, and J. V. Cahn. Metallic phase with long-range orientational order and no translational symmetry. *Phys. Rev. Lett.*, 53:1951–1953, 1984.
- [30] A. Sütő. The spectrum of a quasiperiodic Schrödinger operator. *Comm. Math. Phys.*, 111(3):409–415, 1987.
- [31] A. Sütő. Singular continuous spectrum on a Cantor set of zero Lebesgue measure for the Fibonacci Hamiltonian. *J. Statist. Phys.*, 56(3-4):525–531, 1989.

DEPARTMENT OF MATHEMATICS, RICE UNIVERSITY, HOUSTON, TX 77005, USA

Email address: `damanik@rice.edu`

DEPARTMENT OF MATHEMATICS, VIRGINIA TECH, BLACKSBURG, VA 24061, USA

Email address: `embree@vt.edu`

DEPARTMENT OF MATHEMATICS, TEXAS STATE UNIVERSITY, SAN MARCOS, TX 78666,
USA

Email address: `fillman@txstate.edu`

DEPARTMENT OF MATHEMATICS, DENISON UNIVERSITY, GRANVILLE, OH 43023, USA

Email address: `meim@denison.edu`